Journal of the Geological Survey of Brazil

Neoarchean, Rhyacian and Neoproterozoic units of the Saquinho region, eastern Rio Piranhas-Seridó domain, Borborema Province (northeastern Brazil): implications for the stratigraphic model

Rogério Cavalcante[1]*, Vladimir Cruz de Medeiros[1], Alan Pereira da Costa[1], Jaziel Martins Sá[2], Roberto Ventura Santos[3], Joseneusa Brilhante Rodrigues[4], Alexandre Ranier Dantas[1], Marcos Antônio Leite do Nascimento[2,5], André Luiz Carneiro da Cunha[6]

[1] CPRM - Serviço Geológico do Brasil (NANA/SUREG-RE), Rua Professor Antonio Henrique de Melo, 2010, Natal, RN, Brasil. CEP: 59078-580
[2] UFRN - Universidade Federal de Natal - Departamento de Geologia, Natal, RN, Brasil
[3] UnB - Universidade de Brasíla - Instituto de Geociências, Brasília, DF, Brasil
[4] CPRM - Serviço Geológico do Brasil, SEDE, Brasília, DF, Brasil
[5] UFRN - PPGG, Natal, RN, Brasil
[6] CPRM - Serviço Geológico do Brasil (GEREMI/SUREG-RE), Recife, PE, Brasil

Abstract

Aeromagnetic, petrographic and isotopic data coupled with information obtained from a deep stratigraphic hole (440 m), shallow drillings (<100 m), and field data from the surroundings of the Saquinho iron mine in the Rio-Piranhas-Seridó domain of the Borborema Province, northeastern Brazil, allowed to identify a Neoarchean unit while providing a better understanding of the stratigraphy of the Jucurutu Formation, the host of the iron mineralization, and its basement. The drill hole allowed differentiating three compartments (upper, intermediate and lower). The upper compartment consists of paragneisses/schists, marbles and banded iron formations (top to bottom, respectively) correlated to the Jucurutu Formation (Seridó Group). The marbles provided $\delta^{13}C$ and $\delta^{18}O$ values ranging from 2.4 to 10.4‰ and from -9.7 to -5.3‰, respectively, which are compatible with those of marine-glacial carbonates and correlated to those of the Jucurutu Formation. The intermediate compartment consists of amphibole-bearing biotite augen gneiss, varying in composition from alkali feldspar granite to syenogranite, with U-Pb zircon dating (LAM-MC-ICPMS) of 2210 ± 13 Ma, correlating it with the Rhyacian augen gneisses described in the literature. Finally, the lower compartment consists of a sequence composed mainly of microaugen gneisses, fine banded gneisses and metamafic-metaultramafic rocks (Saquinho Complex). The U-Pb zircon dating (LAM-MC-ICPMS) provided Neoarchean ages of 2512 ± 3 Ma and 2501 ± 3 Ma, respectively, for microaugen gneisses and metamafic-metaultramafic rocks, which were considered as crystallization ages of the protoliths. In the lower part of the drill hole, disseminated sulfides (pyrite, chalcopyrite, and more rarely pyrrhotite) occur, especially in the metamafic-metaultramafic lithotypes, which added to the Neoarchean age of the lithotypes, may represent new economic/metallogenic targets for the Seridó region. The geological model proposed for the iron formations of the Saquinho area involves the interaction of fluids with the Neoarchean mafic rocks, which percolated brittle and/or ductile/brittle structures.

Article Information

Publication type: Regular article
Submitted: 2 February 2018
Accepted: 4 April 2018
Online pub. 20 April 2018
Editor (ad hoc): L.T. Rosa-Costa

Keywords:
Neoarchean,
Saquinho Complex,
Jucurutu Formation,
stratigraphy,
iron ore

*Corresponding author
Rogério Cavalcante
E-mail address:
rogerio.cavalcante@cprm.gov.br

1. Introduction

The Seridó region, in the Borborema Province, is one of the main metallogenic provinces of Brazil, with important deposits of tungsten, gold, iron, tantalum, niobium, and gems (Beurlen 1995; Biondi 2003; Cavalcante et al. 2015). The mineral activity in this region dates back to more than 70 years ago, being one of the largest tungsten producers in the country, with emphasis on mines in the Currais Novos, Bodó and Lajes regions, in Rio Grande do Norte (Salim 1979, 1993; Maranhão et al. 1986; Souza Neto et al. 2008). This mineral abundance has been attributed to several factors including tectonic setting, structural relations, mineralizing systems, intrusive bodies related to the source of mineralizing fluids, and the presence of fertile Archean rocks.

Dantas et al. (2014) and Ruiz et al. (2018) demonstrated the contribution of Archean material to basement gneissic rocks and metaultramafic rock lenses in the vicinity of western São Tomé and Bonfim mine (in Lajes, Fig. 1), respectively. The U-Pb zircon dates indicated Paleoarchean ages for these rocks. Costa et al. (2014) suggested that their presence might be associated with the origin of the Fe-Ti-V oxide mineralizations in the region. Thus, it is important to map and improve the knowledge on the distribution of Archean portions in the region since these terrains can be strong indicators of the metal potential.

In the Saquinho region, there are questions regarding the existing iron and carbonate formations as whether they represent Ediacaran supracrustal sequences (Jucurutu Formation of the Seridó Group) or older units, as well as their stratigraphic positioning.

https://doi.org/10.29396/jgsb.2018.v1.n1.2
ISSN: 2595-1939

Most of the data presented here are from a stratigraphic borehole in the Saquinho region (FD-SE-002) located 20 km northwest of the municipality of Cruzeta, in the central portion of Rio Grande do Norte. The drilling performed by the CPRM- Geological Survey of Brazil aimed at investigating the lithotypes of the Jucurutu Formation (Pessoa 1986; Medeiros et al. 2012a), the iron ore host of the Saquinho mine, and exploring the possibility of stratigraphic repetition of the Seridó Group/basement. As such, we performed the lithostratigraphic/structural characterization of the Jucurutu Formation in the Saquinho region, analyzed the nature of the contact between the metasediments of the Seridó Group and its basement, evaluated the presence of metamafic-metaultramafic rocks, and finally, presented a stratigraphic model for the studied region, besides suggesting processes responsible for the genesis of the iron ore in Saquinho.

2. Regional geology

The study site is located in the northeastern Borborema Province as defined by Almeida et al. (1981). In recent years, some authors have proposed a tectonic framework (totally or partially) for the Province, based on the concept of tectonostratigraphic terrain and/or domains (Jardim de Sá et al. 1992; Santos 1996; Jardim de Sá 1994; Van Schmus et al. 1995; Brito Neves et al. 2000; Santos et al. 2000). The area is inserted in the Rio Piranhas-Seridó Domain, bordered by the Portalegre and Picuí-João Câmara Shear Zones to the west and east, respectively. To the north, it is covered by Mesozoic (Potiguar Basin) and Cenozoic sediments, while the southern limit is defined by the Patos Lineament (Fig. 1).

The Rio Piranhas-Seridó Domain consists essentially of the Caicó Complex (Ebert 1969; Jardim de Sá 1984; Brito Neves et al. 2000) of Rhyacian age (Dantas 1988; Souza 1991; Jardim de Sá 1994; Souza et al. 2007, 2016), Siderian orthogneisses and migmatites of the Arabia Complex (Costa and Dantas 2014), Rhyacian augen gneisses (Hollanda et al. 2011; Medeiros et al. 2012b), the Seridó Group (Jardim de Sá and Salim 1980; Jardim de Sá 1984, 1994) representing Ediacaran supracrustal sequences (Van Schmus et al. 2003; Holanda et al. 2015), and Ediacaran granitoids associated with the Brasiliano magmatism (see review in Nascimento et al., 2015) (Fig. 1). Recently, the presence of Paleoarchean rocks associated with the mineralization of the Bonfim/Lajes and São Tomé regions (Fig. 1) has been reported in more restricted areas in this domain by Dantas et al. (2014) and Ruiz et al. (2018), suggesting the important role of Archean sources in the mineralizing process.

The São José do Campestre Domain has Rhyacian gneisses and migmatites, lithotypes of the Seridó Group and Ediacaran granitoids, in addition to a large volume of Archean units (Fig. 1), as pointed out by Dantas (1996), Dantas et al.

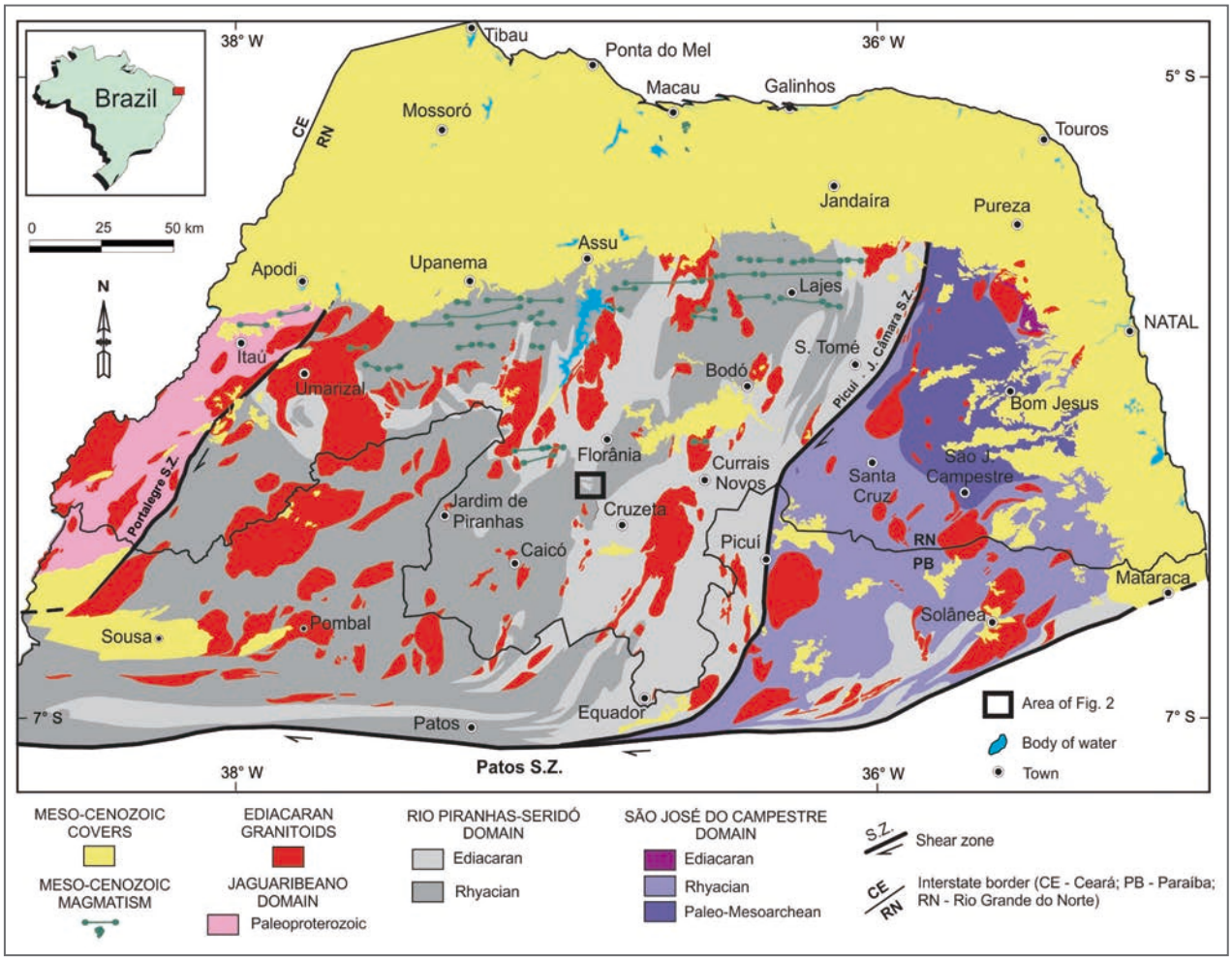

FIGURE 1 - Geological framework of northeastern Borborema Province showing the studied area. Modified from Medeiros et al. (2017).

(1997, 2004, 2013), Dantas and Roig (2013), Roig and Dantas (2013), and Souza et al. (2016).

This set of rocks have undergone intense Ediacaran granitogenesis, which is generally associated with extensive transcurrent shear zones (Jardim de Sá 1994; Dantas 1996; Nascimento et al. 2015).

In the study site and adjacencies, Medeiros et al. (2012a) and Cavalcante et al. (2016) mapped units of the Caicó Complex, augen gneisses (Rhyacian) and the Jucurutu Formation (Fig. 2) while more recent studies on the iron units were presented by Campos (2011), Sial et al. (2015) and Dantas et al. (2017).

The Caicó Complex consists mainly of Rhyacian orthogneisses, migmatites and metasupracrustal rocks (2.25 to 2.10 Ga), considering the U-Pb zircon ages obtained for ortho-derived rocks of this complex by Hackspacher et al. (1990), Legrand et al. (1991), Dantas (1992) and Souza et al. (2016).

The augen gneisses are generally granitic, representing a transitional suite with signature between alkaline and potassic calc-alkaline (Medeiros et al. 2012b). Hollanda et al. (2011) and Medeiros et al. (2012b) determined (U-Pb in zircon) Rhyacian ages (2.25 to 2.15 Ga). These are representatives of the Poço da Cruz suite defined by Ferreira (1998) and in part of the G2-type granitoids referred to by Jardim de Sá et al. (1981) and Jardim de Sa (1994).

The Seridó Group comprises, from base to top, the Jucurutu (paragneisses with intercalating marbles, calc-silicate rocks, micaschists, metavolcanic rocks and iron formations), Equador (quartzite and metaconglomerate), and Seridó (predominant micaschists with rare intercalating marble, metavolcanic and calc-silicate rocks) formations as proposed by Jardim de Sá and Salim (1980), Jardim de Sá (1984, 1984), the latter admitted in the present work. Hollanda et al. (2015) suggest an alternative stratigraphic positioning for these units, considering the Equador Formation as an older unit.

U-Pb ages in detrital zircons of rocks from the Seridó and Jucurutu formations obtained by Van Schmus et al. (2003) and Hollanda et al. (2015), indicated the end of the Neoproterozoic (Ediacaran) as the sedimentation period for these two formations.

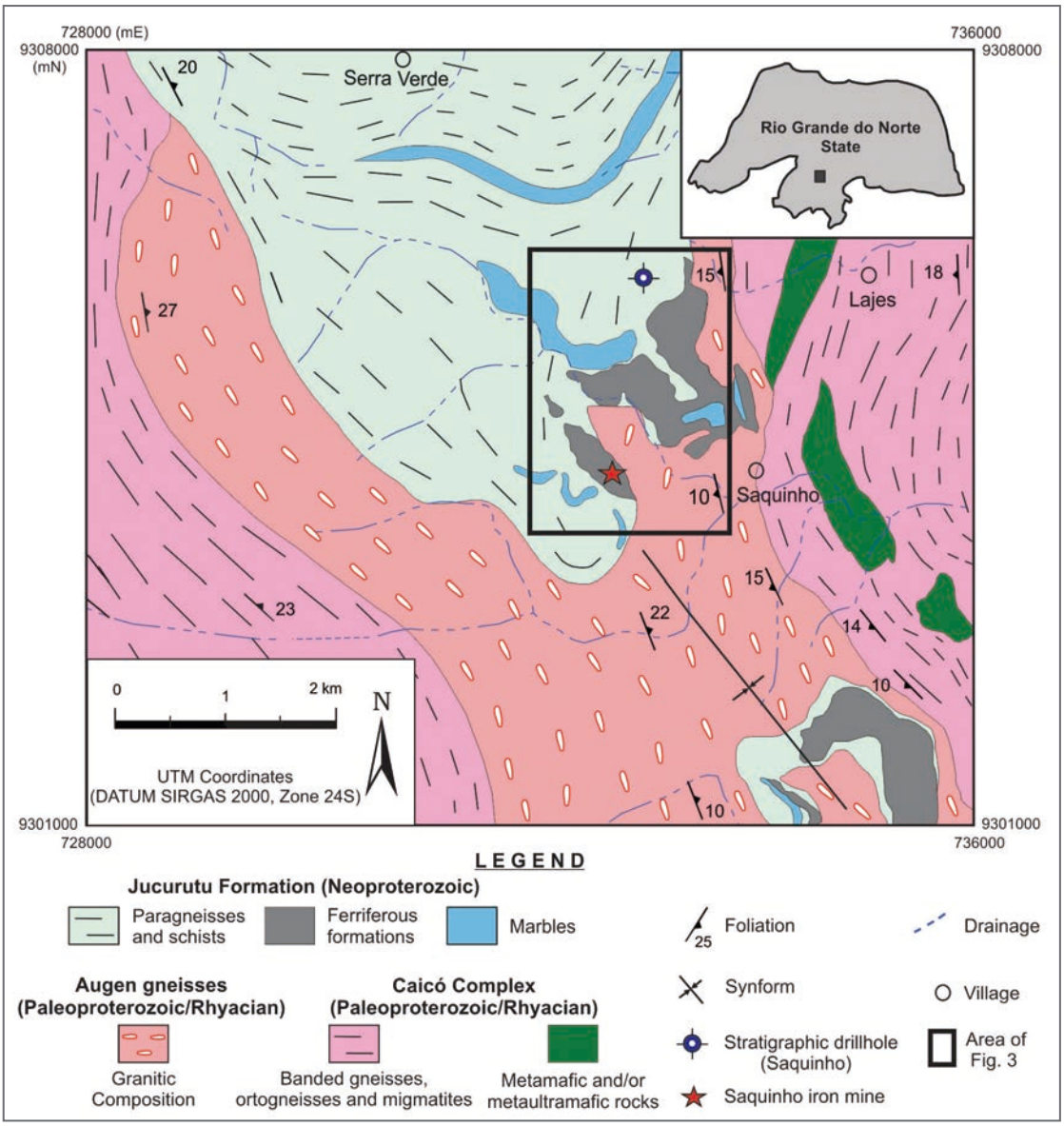

FIGURE 2 - Geological map of the Saquinho-Serra Verde region, adapted from Medeiros et al. (2012a).

3. Sampling and analytical procedures

The samples were obtained from the Saquinho region outcrops and from the FD-SE-002 drilling hole (Fig. 2) performed in the homonymous iron mine. The drill-core samples were oriented every 30 meters (approximately), allowing to obtain the structural parameters, and correlating them with the field data, logging and determining the geological profile of the borehole, following the methodology described by Medeiros et al. (2017) for a stratigraphic hole in the Currais Novos region (Fig. 1).

Petrographic analyses were performed at several borehole intervals to characterize the lithologies, while the whole rock C and O isotopic compositions were determined in the carbonate layer with a more homogeneous mineralogical constitution (purest marbles). The U-Pb zircon determinations were conducted in three samples (granitic augen gneiss, monzogranitic microaugen gneiss, and metagabbronorite), collected in drill-core, to define the chronology of the geological events.

Isotopic data ($\delta^{13}C$ and $\delta^{18}O$) were obtained at the Laboratory of Stable Isotopes of the Universidade of Brasília (UnB), where the isotopic composition of carbon and oxygen was determined by continuous flow Isotope Ratio Mass Spectrometry (IRMS) and gaseous source with a DELTA V PLUS (Thermo®) magnetic sector and double entry. For the analyses, the Thermo® GasBench II accessory was used to insert 300µg of sample into clean glass bottles closed with rubber septum caps, which were stored in a block at a controlled temperature of 72ºC. A gas chromatography needle is then used to perform the so-called flushfill process for exchanging the flask atmospheric air by injecting a continuous helium stream for 5 min to render the reaction medium inert. A metering pump is used to insert five drops of 100% H_3PO_4 into each flask, allowing the CO_2 extraction reaction to occur for one hour. After CO_2 extraction, a second chromatographic needle collects the gas, sending it to a chromatographic column for separation using helium as a carrier; the gas is then injected into the source of ions for the isotopic measurements. The $\delta^{13}C$ and $\delta^{18}O$ values are expressed as per thousand (‰) based on the Vienna Pee Dee Belemnit (V-PDB) and Vienna Standard Mean Ocean Water (V-SMOW) standards, respectively. The analytical errors are 0.05 and 0.10‰ for $\delta^{13}C$ and $\delta^{18}O$, respectively.

For the U-Pb zircon study, the crystals were separated after crushing, sieving (<500µ) and heavy minerals concentration via panning in the Grinding Laboratory of the Department of Geology of the Universidade Federal do Rio Grande do Norte (DG/UFRN). Subsequently, a Frantz Magnetic Separator was used to separate the non-magnetic minerals, of which the zircon fractions were separated manually using a binocular loupe to select clear minerals with no visible inclusions. The crystals were mounted using double-sided tape, embedded in epoxy resin (cold), worn out for exposing the inside of the grains and polished with 0.25 µm diamond paste, followed by ultrasound bath in dilute nitric acid (3%), Nanopure® water, and finally in acetone to extract any residual moisture. The analyses were conducted in the Laboratory of Geochronology of the UnB, following the procedure described by Buhn et al. (2009).

The isotopic determinations were performed on the LAM-MC-ICP-MS Neptune (Thermo-Finnigan) spectrometer coupled to the Nd-YAG (λ = 213nm) Laser Ablation System (New Wave Research, USA). The ablation occurred in 25-40 µm spots, at 10 Hz frequency and 0.19 to 1.02 J/cm^2 fluence. The pulverized material was carried by He (~0.40 L/min) and Ar (~0.90 L/min) flow. The GJ-1 international standard was used for correcting equipment drift and the fractionation between the U and Pb isotopes. Analyses were also performed in the international standard zircon 91500 to verify accuracy. The data were acquired in 40 cycles of 1 second while the collection procedure followed the reading sequence: 1 blank, 1 standard, 4 samples, 1 blank and 1 standard. The intensities of the ^{202}Hg, $^{204}(Pb+Hg)$, ^{206}Pb, ^{207}Pb, ^{208}Pb and ^{238}U masses were determined at each reading. The raw data, including blank corrections, equipment drift and common lead, were reduced using the tools of the Chronus software in Excel (Oliveira 2015). The ages were calculated and the Concordia diagrams were plotted using ISOPLOT 3.0 (Ludwig 2003).

4. Results

4.1. Surface geology of the Saquinho area

The geology of the Saquinho mine area (Fig. 3) consists of Rhyacian biotite augen gneisses, superimposed by schists, paragneisses, banded iron formations and marbles of the Jucurutu Formation. Cover/soil and colluvial deposits correspond to younger units.

The biotite augen gneisses with amphibole occur in the southern and eastern regions (Fig. 3), displaying granitic composition, pinkish to grayish color, and coarse grain (Fig. 4A). The porphyroclastic texture is given by potassic feldspar crystals up to 5 cm long, which define a mineral stretching lineation with a low angle plunge (Fig. 4A).

Quartz-chlorite-biotite schists, locally with garnet, outcrop in the central and eastern portions of the area (Fig. 3). These are gray to yellowish rocks, with grano-lepidoblastic texture, and a prominent foliation marked by phyllosilicates.

The banded iron formations occurring in the central and eastern areas (Fig. 3) are characterized by an ocher-reddish soil.The lithotypes alternate laminations rich in quartz and magnetite+hematite, magnetite+hematite+amphibole, magnetite+hematite+sulfide, and more rarely magnetite +carbonate.

The marbles that crop out in the western and mid-eastern areas (Fig. 3) are granoblastic with medium grain, consisting essentially of whitish, and more rarely gray, calcite forming alternating white and grayish levels (Fig. 4C).

The amphibole-biotite schists with garnet are restricted to a single outcropping body in the eastern region (Fig. 3), and show green to greenish-gray colors.

Biotite (amphibole) paragneisses crop out in the western and northeast portions of the area (Fig. 3). They are medium-grained lepidogranoblastic, colored bluish-gray with gneissic banding that alternates quartz+feldspar and biotite±amphibole±magnetite levels (Fig. 4D).

4.2. Stratigraphic compartments

The lithologies intercepted by the drilling hole (FD-SE-002) can be grouped into three large compartments (Fig. 5), from top to bottom, as metasedimentary rocks (Jucurutu Formation), granitic augen gneisses (Rhyacian), and a succession of

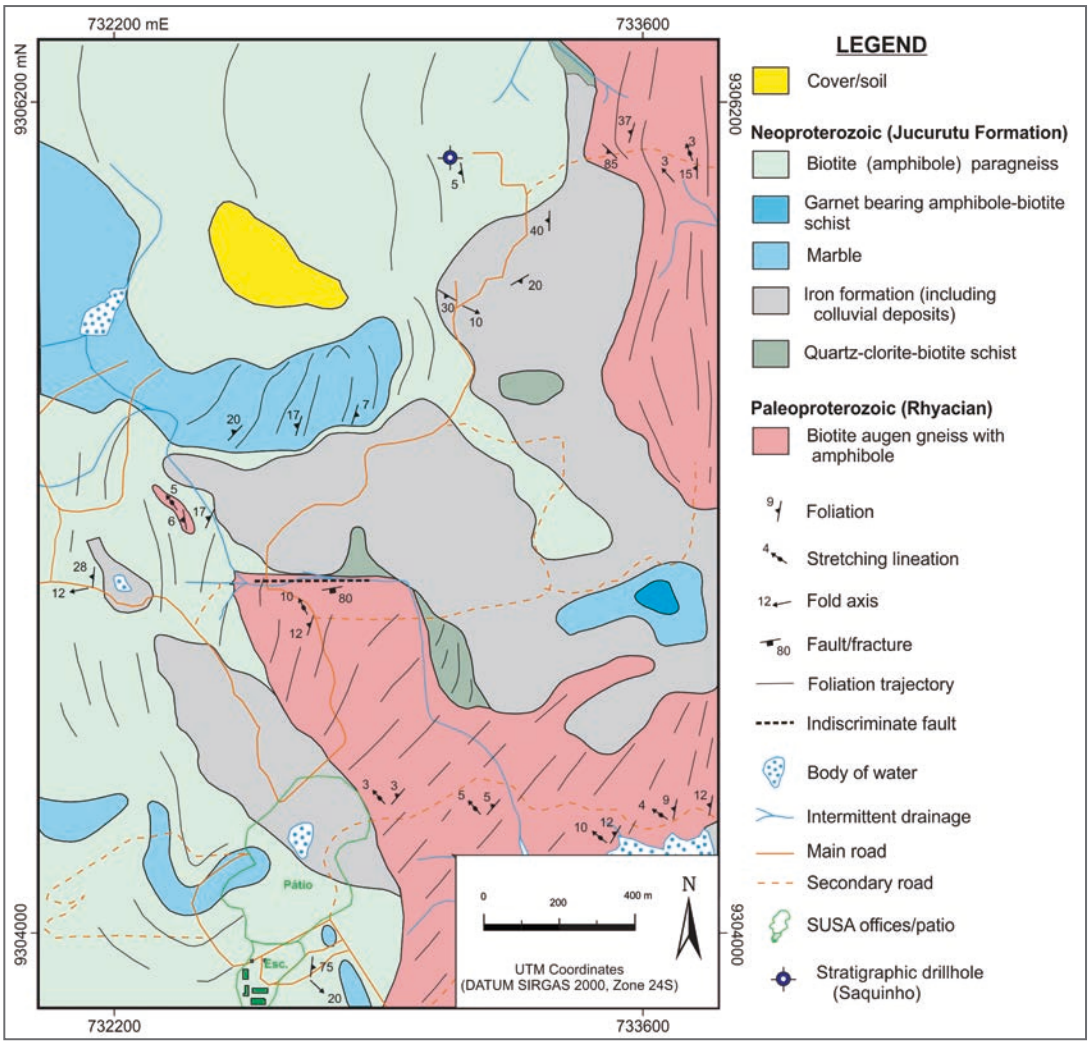

FIGURE 3 - Geological map of the northern portion of the Saquinho iron mine, adapted from the data provided by Susa Indústria e Comércio de Produtos Minerários Ltd.

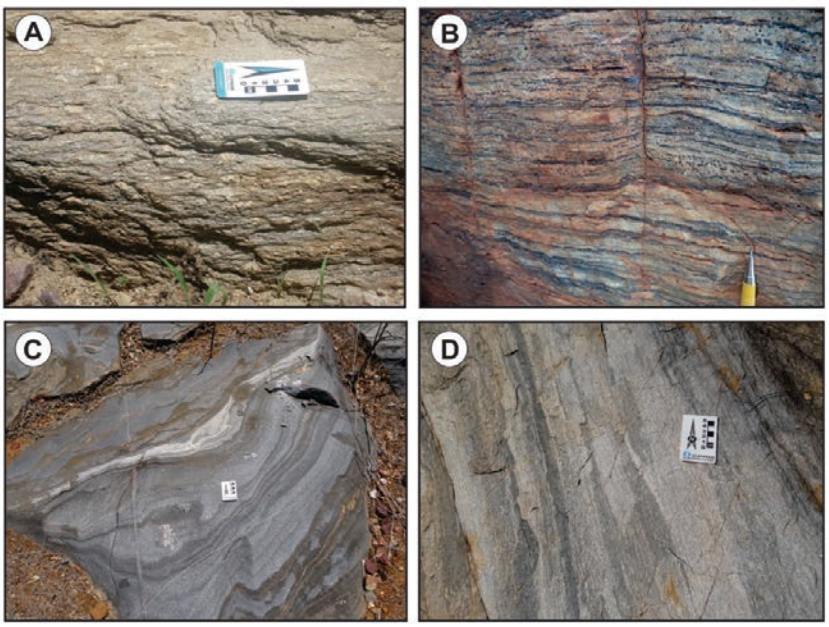

FIGURE 4 - Field features of the rocks around the Saquinho mine: (A) augen gneiss with stretching lineation given by potassic feldspar crystals; (B) banded iron formation; (C) marble with banding formed by white, light and dark gray levels; (D) biotite (amphibole) paragneiss with alternating whitish and light gray bands.

metamafic-ultramafic felsic gneissic rocks intercalated by porphyroclastic orthogneisses (Saquinho Complex). The contact is nonconforming and/or tectonic between the upper and intermediate compartments, and abrupt, between the intermediate and lower compartments.

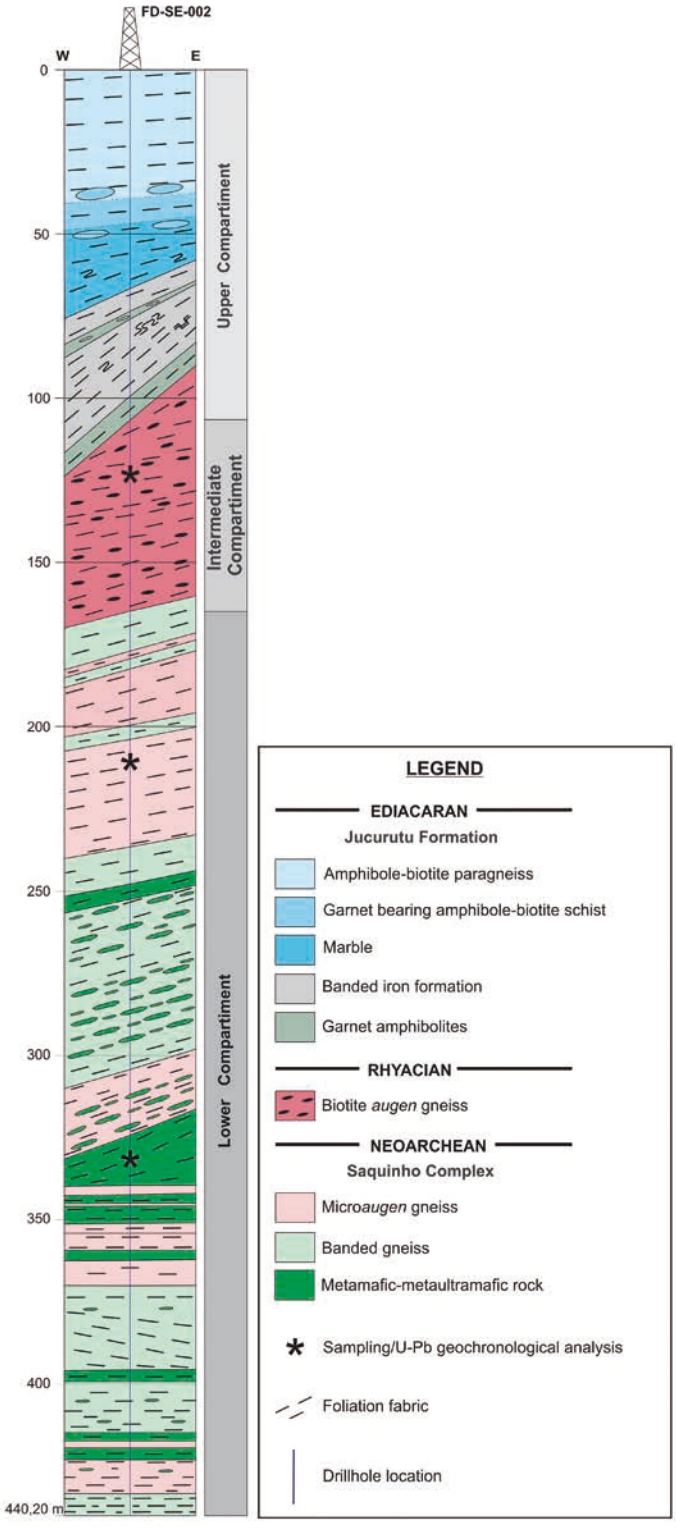

FIGURE 5 - Cross-section of the drill hole FD-SE-002 performed near the Saquinho iron mine, highlighting the three geological compartments, as well as the sampling sites for the U-Pb geochronological analyses.

4.2.1. Upper compartment (Jucurutu Formation)

Compartment associated with the Jurucutu Formation (0.0 to 107.9m deep, Fig. 5), where biotite paragneisses, amphibole-biotite schists with garnet, marbles, banded iron formations, chlorite-biotite schists and garnet amphibolites occur.

The biotite paragneisses are fine lepidogranoblastic rocks of gray color, constituted by quartz-feldspathic levels and levels rich in biotite, magnetite, and ±amphibole. They are composed of quartz (45-55%), biotite (12-20%), plagioclase (5-15%), potassium feldspar (5-15%), amphibole (5-15%), muscovite (1-10%), epidote (3-6%), opaque minerals (1-8%), titanite (1-3%) and apatite (<1-2%).

The marbles are granoblastic and fine- to medium-grained, with light and dark gray bands, millimeter to centimeter thick (Fig. 6A). The rocks are formed by calcite (62-87%), biotite (1-18%), amphibole (1-10%), feldspars (2-6%), quartz (<1-10%), pyroxene (2 -7%), opaque minerals (<1-7%), and white mica (<1-2%) (Fig. 6C).

The iron formation consists of two facies, oxide (Fig. 6B) and silicate. The petrographic data (Figs. 6D and 6E) show that the first is represented by fine- to medium-grained granoblastic rocks, with a whitish and greenish-black banding, consisting of quartz (20-34%), magnetite (10-25%), amphibole (15-60%), garnet (2-12%), chlorite (<1-15%), chalcopyrite (1-4%), pyrite (1-6%), and pyroxene (≤1%). The second facies is medium-grained and grano-nematoblastic, colored whitish to grayish black, alternating quartz (36-55%), magnetite (8-40%), hematite (≤22%), amphibole (≤15%), chlorite (≤4%), muscovite (<1-2%), pyroxene (≤1%), and pyrite (≤1%).

4.2.2. Intermediate compartment (augen gneisses)

The intermediate compartment (107.9 to 165.1m deep, Fig. 5) consists of an augen gneiss, pinkish to off-white, inequigranular from medium to coarse grain, formed by porphyroclasts of potassium feldspar and plagioclase immersed in a gray to whitish matrix, sometimes with mylonitic texture. They have a penetrating gneiss banding and a well-marked lineation of feldspar porphyroclasts (Fig. 7A). The composition ranges from alkali feldspar granite to syenogranite, consisting of microcline (26-51%), quartz (12-39%), biotite (8-25%), plagioclase (1-12%), amphibole (1-8%), opaque minerals (1-6%), titanite (1-4%), and epidote (2-3%). The fabric is marked by quartz and feldspar augen (Fig. 7B) bordered by biotite crystals, defining the rock foliation.

4.2.3. Lower compartment (Saquinho Complex)

The third compartment (165.1 to 440.2 m deep, Fig. 5) includes a group of rocks that alternates three main lithotypes, microaugen gneisses, banded gneisses and metamafic (meta-ultramafic?).

The microaugen gneisses correspond to a rock sequence with very fine to medium grain (felsic meta-subvolcanic rock?) and feldspar porphyroclasts (Fig. 8A). They are predominantly monzogranitic, foliated, with incipient banding, constituted by a medium to fine matrix colored pink, light and dark gray. Microscopically, few feldspar agglomerates are observed as microaugen (Fig. 8D). They consist of plagioclase (18-24%), quartz (27-38%), microcline (20-26%), biotite (8-20%), epidote (<1-12%), and opaque minerals (2-3%), as well as traces of titanite and apatite.

The gneiss banding varies from millimeter to centimeter thick, and consists of a fine to medium matrix composed of different felsic and mafic levels (Figs. 8B and 8E). The former are light gray and present crystals of quartz (10-33%), plagioclase (12-26%) and microcline (3-38%). The latter are dark gray, formed by the mafic minerals, amphibole (40-50%), biotite (15-20%), and pyroxene (1-12%). The felsic levels are monzogranitic while the most mafic have a amphibole-gabbro to amphibole-tonalite composition.

In this compartment, there is a group of metamafic-metaultramafic rocks of greenish coloration, medium- to coarse-grained, composed essentially of amphiboles/pyroxenes that constitute the amphibolite and gabbroic varieties (Figs. 8C and 8F).

Petrographically, they are classified as biotite-pyroxene-amphibole metamafic rocks, constituted by amphiboles (22-65%), most of which are formed from pyroxenes indicating a protolith of ultramafic composition, pyroxenes (10-22%), biotite (8%), plagioclase (3-15%), quartz (0-3%), chlorite (<1-28%), epidote (1-5%), magnetite (1-4%), pyrite (1-3%), and chalcopyrite (1-2%).

4.3. Structural features

Medeiros and Dantas (2015) stated that the rocks of the Saquinho region and neighboring areas were affected by at least three phases of ductile (D1, D2, and D3) and brittle deformations. The first one (D1) is evidenced only in the Paleoproterozoic/Rhyacian (augen gneisses/Caicó Complex) lithotypes to the north, outside the studied area, while the last two (D2 and D3) were also evidenced in Neoproterozoic lithotypes (Jucurutu Formation).

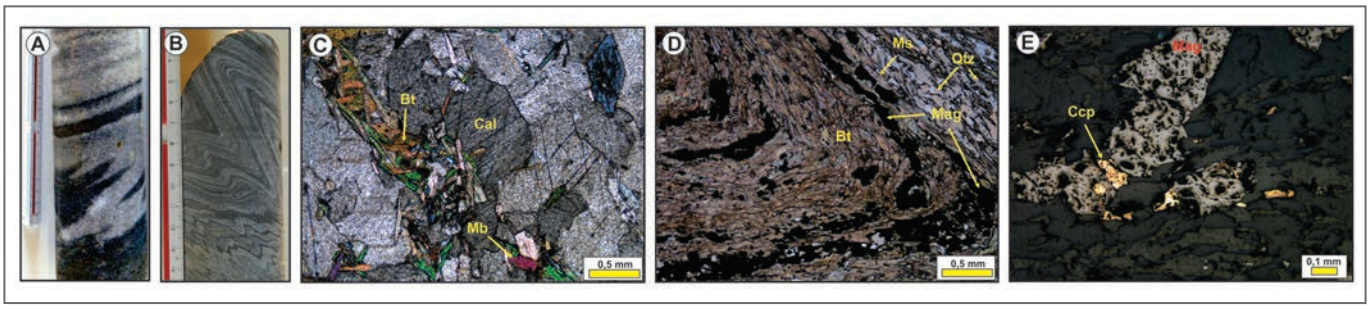

FIGURE 6 - Petrography of the upper compartment (Jucurutu Formation) units: (A) marble drill core showing interdigitation of light and dark gray beds; (B) chevron-like folds in drill-core of the banded iron formation; (C) photomicrograph of marble formed by calcite, biotite and muscovite (crossed Nicols); (D) photomicrograph of the banded iron formation evidencing a hinge zone of a tight fold delineated by alternating quartz+phyllosilicates and magnetite (parallel Nicols); (E) magnetite crystal with chalcopyrite at the edges (reflected light). Bt = biotite, Cal = calcite, Ccp = chalcopyrite, Mag = magnetite, Mb = white mica, Qtz = quartz.

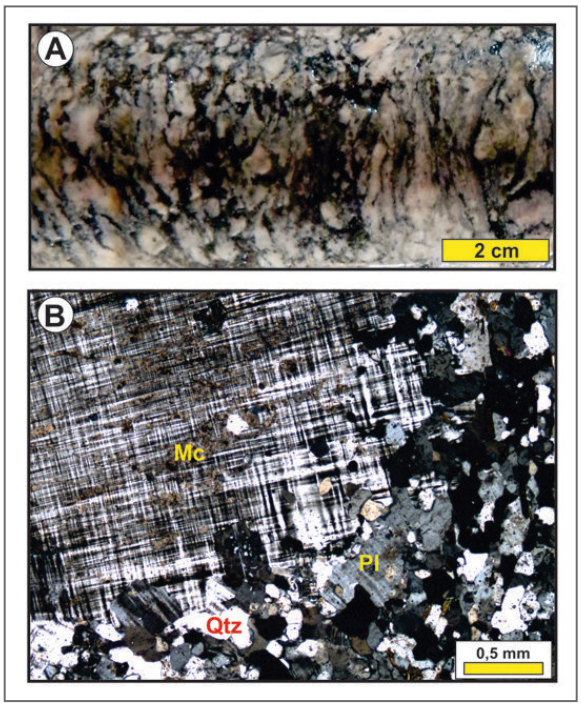

FIGURE 7 - Textural characteristics of the augen gneiss of the intermediate compartment. (A) drill-core showing the porphyroclastic texture; (B) photomicrograph showing microcline porphyroclasts immersed in mortar texture of quartz-feldspathic composition (crossed Nicols). Mc = microcline, Pl = plagioclase, Qtz = quartz.

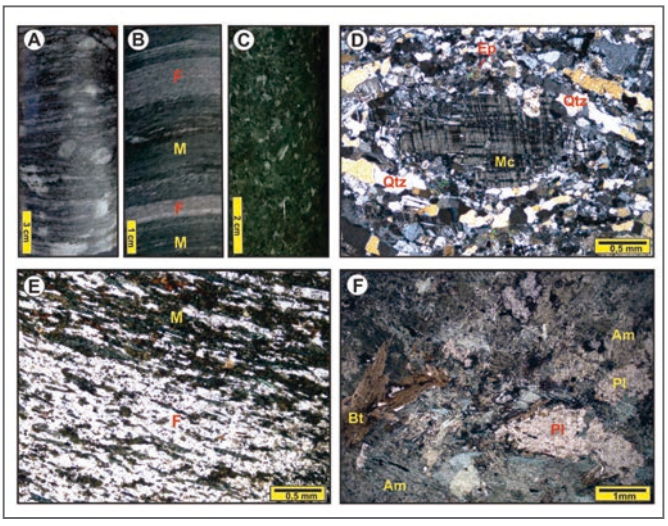

FIGURE 8 - Petrographic features of the lower compartment units: drill-cores showing porphyroclastic texture marked by feldspars in microaugen gneiss (A), mafic and felsic levels of banded gneiss (B) and thick inequigranular texture of metagabbronorite (C); (D) photomicrograph of microaugen with microcline porphyroclasts in quartz-feldspathic matrix (crossed Nicols); (E) photomicrograph of the banded gneiss (parallel Nicols) showing the alternation between the mafic (amphibole schist) and felsic (amphibole gneiss) phases; (F) photomicrograph of metamafic rock showing the mafic phases with amphibole and biotite, and felsic phases with plagioclase (parallel Nicols). Am = amphibole, Bt = biotite, Ep = epidote, Mc = microcline, Pl = plagioclase, Qtz = quartz. M = mafic band, F = felsic band.

The D2 event generated an originally low-angle foliation (S2) , which is, in some places, associated with a high rake stretching lineation (Fig. 4A), suggesting a contractional tectonic with NW vergence. Sometimes recumbent folds formed during this event are also observed. A gentle synform with a 125°Az sub-horizontal axis and a sub-vertical axial plane, associated with the D2 event, was generated in the southeast portion of the studied area (Fig. 2), affecting the Rhyacian augen gneisses and lithotypes of the Jucurutu Formation, indicating that this folding is from the Ediacaran period.

Steeply-dipping NE-SW trending transcurrent shear zones, associated with the D3-phase, were observed at the outcrop scale and regionally northeast of the studied region, as well as generally open folds with a sub-vertical axial surface and a gently-dipping NE-NW axis.

The brittle deformation (faults and/or fractures), late- or post-D3, is commonly evidenced in both the lithotypes of the Jucurutu Formation (Fig. 9) and the Rhyacian augen gneisses. Faults presenting normal displacement were observed the pit of the Saquinho mine (Fig. 9A), and in the drill-core, being the latter expressed by the displacement of carbonate and/or quartz veins in amphibole-granite-biotite paragneiss/schist (Fig. 9B) and in quartz veins in banded iron formations (Fig. 9C).

The fault/fracture direction oscillates between 0º and 40ºAz predominantly, with steep dips to east-southeast in the western portion of the Saquinho ore deposit, and west-northwest in the eastern part, which are consistent with the data reported by Pessoa (1986). These features, along with the associated kinematic markers, indicate an architecture similar to a system of normal faults.

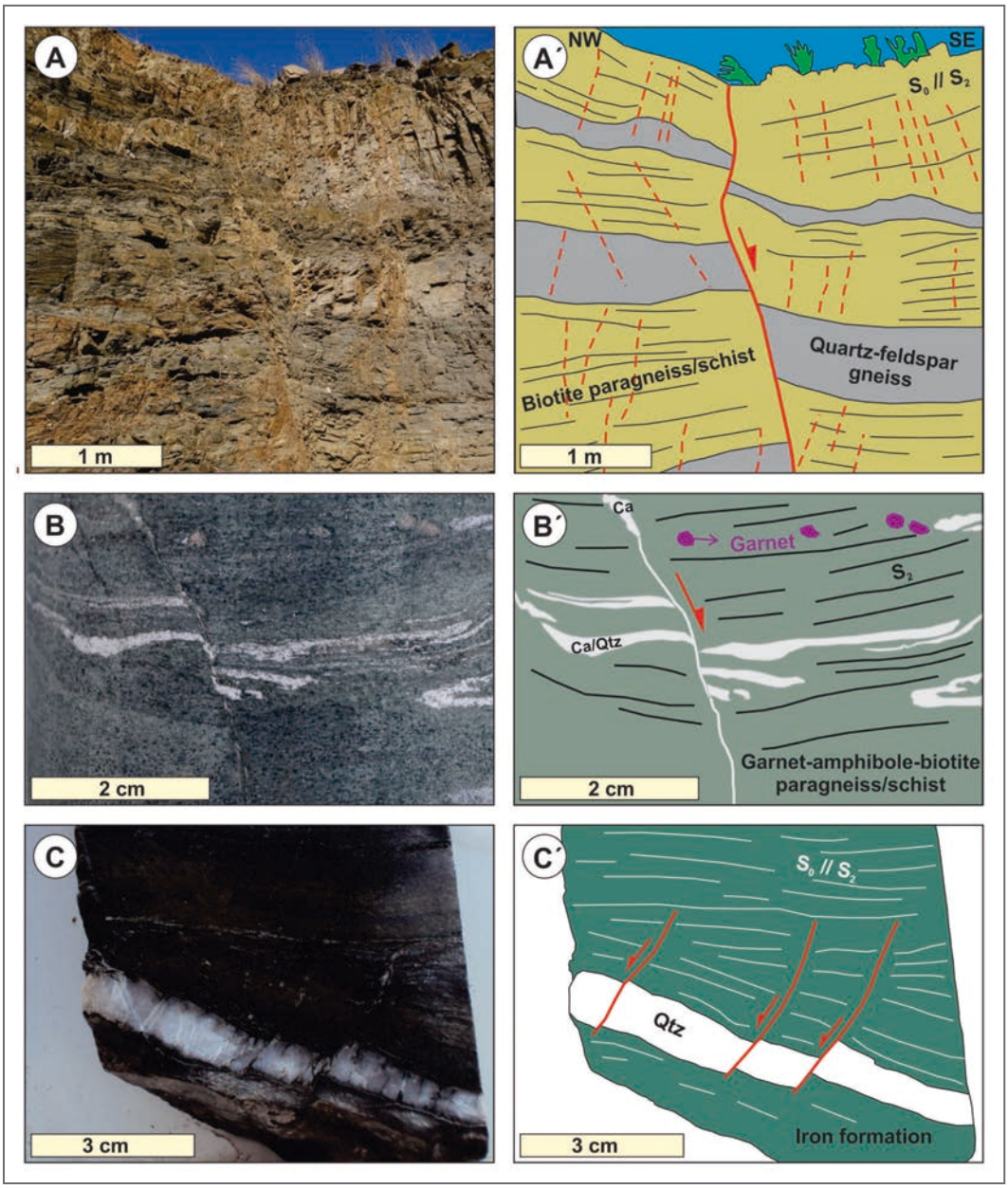

FIGURE 9 - Photos of structural features of the brittle regime in the rocks of the Jucurutu Formation, in the Saquinho mine region (A, B, and C) and respective interpretative drawings (A', B', and C'). (A) Subvertical fault (80°/50°Az) affecting paragneiss and iron formation in an open pit operation; (B) and (C) drill-cores showing normal faults with centimeter heave superimposed on paragneiss/schist (B) and iron formation (C). Qtz = quartz; Ca = carbonate (calcite).

4.4. C and O isotopes

The C and O isotopic compositions were determined in the marbles as to correlate them with those of the Jucurutu Formation already studied by Nascimento et al. (2004, 2007), Campos (2011), Figueiredo (2012) and Sial et al. (2015). The $\delta^{13}C$ and $\delta^{18}O$ values were determined in fifteen marble samples collected between 47 and 66 meters deep, from the Saquinho borehole (Table 1).

All the analyzed samples correspond to light gray, calcitic granoblastic marbles, with $\delta^{13}C$ values between 2.4 and 10.4‰, and $\delta^{18}O$ between -9.7 and -5.3‰ (Table 1 and Fig. 10)

The $\delta^{13}C$ and $\delta^{18}O$ values available in the literature for the studied region (Nascimento et al. 2007; Campos 2011; Figueiredo 2012; Sial et al. 2015) show that $\delta^{13}C$ values for the Jucurutu Formation marbles are generally positive and tend to be constant when the original composition of the rock is preserved (Fig. 11). Whereas the marbles of the Seridó

TABLE 1 - Whole-rock isotopic compositions (C and O) determined in samples of the Saquinho borehole marbles (FD-SE-002).

SAMPLE	DEPTH (m)	$\delta^{13}C$‰ (V-PDB)	$\delta^{18}O$‰ (V-PDB)	$\delta^{18}O$‰ (V-SMOW)
FD-SE-002 (15933)	47.60	10.20	-9.74	20.82
FD-SE-002 (15934)	48.60	10.43	-8.47	22.13
AR-R-010 (14633)	49.62	4.59	-6.23	24.43
FD-SE-002 (15935)	51.00	4.23	-7.25	23.39
FD-SE-002 (15936)	52.50	6.16	-6.19	24.48
AR-R-011 (14634)	53.90	2.40	-8.60	21.99
FD-SE-002 (15937)	55.00	7.64	-5.35	25.34
FD-SE-002 (15938)	56.00	4.51	-6.39	24.28
FD-SE-002 (15939)	57.25	5.45	-5.71	24.97
AR-R-012 (14635)	58.03	5.10	-6.69	23.96
FD-SE-002 (15940)	61.35	5.01	-7.77	22.85
FD-SE-002 (15941)	62.60	3.72	-8.42	22.18
FD-SE-002 (15942)	63.65	4.66	-9.23	21.35
AR-R-013 (14636)	64.30	4.39	-8.61	21.99
FD-SE-002 (15943)	66.00	5.35	-9.44	21.13

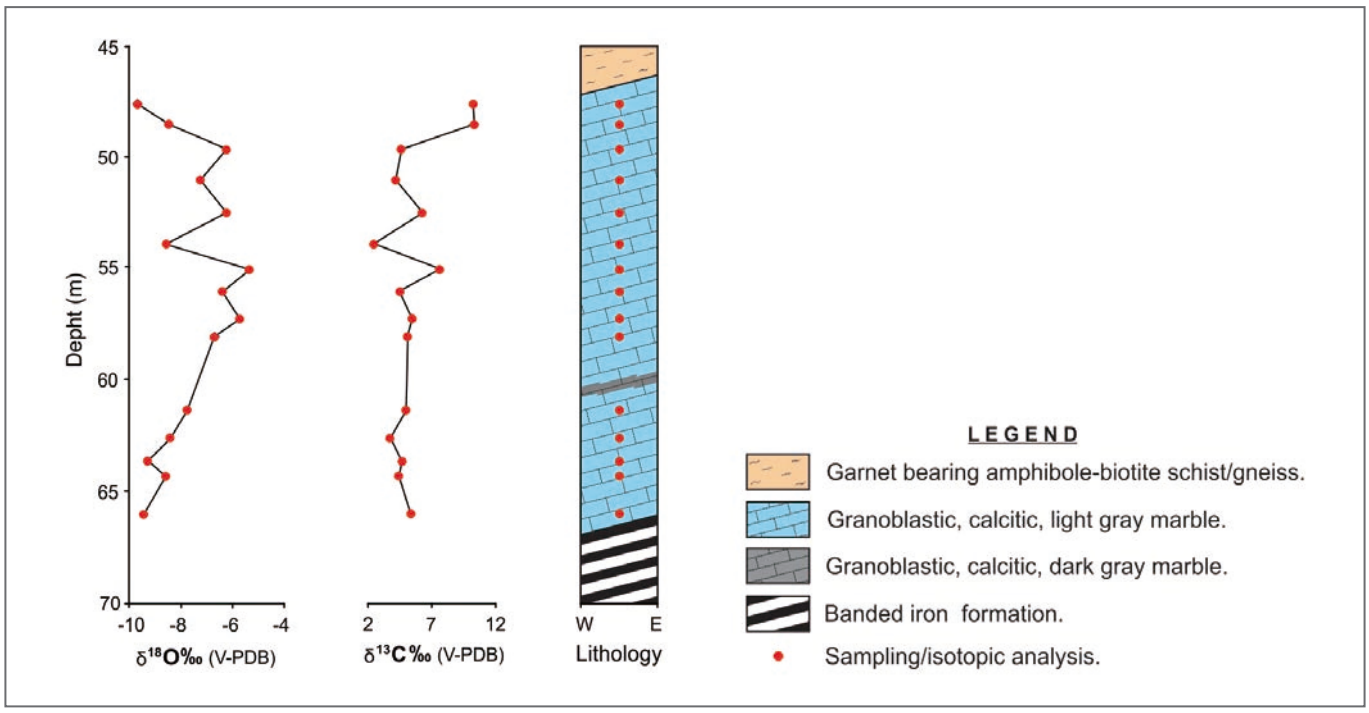

FIGURE 10 - Isotopic (C and O) chemostratigraphy of the marbles of the Saquinho stratigraphic hole, using data from Table 1.

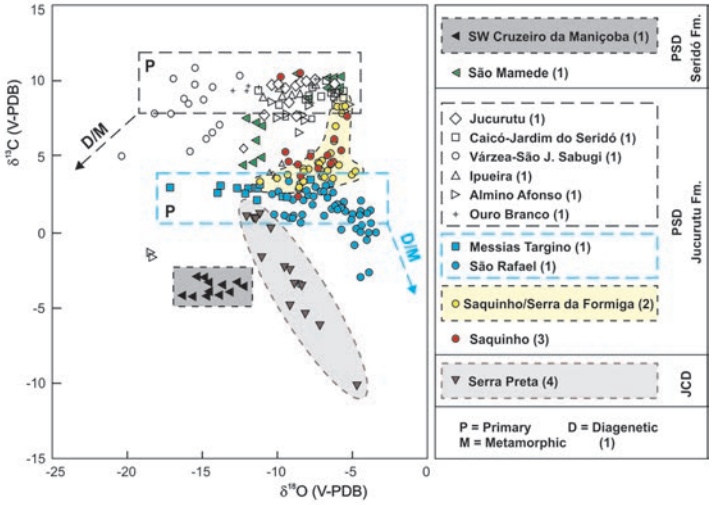

FIGURE 11 - Distribution diagram of O and C isotope compositions of the marbles of the Rio Piranhas-Seridó/PSD Domain (Jucurutu and Seridó formations) and the São José do Campestre/JCD Domain (Serra Preta/Serra Caiada Complex). Data source: (1) Nascimento et al. (2007) and Sial et al. (2015); (2) Campos (2011) and Sial et al. (2015); (3) this work; (4) Figueiredo (2012).

Formation present positive (São Mamede) and negative values (SW of Cruzeiro da Maniçoba-Currais Novos).

The available analyses for the marbles of the Serra Preta region (Figueiredo 2012), inserted in the São José do Campestre Domain (Serra Caiada Complex), of Archean age (Dantas 1996; Dantas et al. 2004, 2013; Dantas and Roig 2013; Roig and Dantas 2013; Souza et al. 2016), have slightly positive to moderately negative $\delta^{13}C$ values (+1.2 to -10.2‰) and a negative correlation with $\delta^{18}O$ (Fig. 11).

The $\delta^{13}C$ and $\delta^{18}O$ values obtained in this work and in the literature suggest that the Saquinho marbles can be correlated with those of the Jucurutu Formation (Fig. 11) and, consequently, with the deposition in a marine-glacial environment, corroborating the models proposed by Nascimento et al. (2007) and Sial et al. (2015) for this unit.

4.5. U-Pb zircon dating

Drill-cores of the intermediate (granitic augen gneiss) and lower (monzonitic microaugen gneiss and meta-gabbronorite of the Saquinho Complex) compartments were collected from the Saquinho borehole to obtain their crystallization age, considered as representative of the basement of the supracrustal sequence of the Jucurutu Formation (Fig. 5).

4.5.1. *Augen* gneiss

The amphibole-bearing biotite augen gneiss with granitic composition was sampled between 121.0 and 122.0 meter deep (Fig. 5). The zircon grains (Fig. 12) are generally elongated prismatic, about 150-200 µm long (length/width = 2.6 to 3.1), usually with growth zonation (concentric) along the rims. The scanning electron microscope (SEM) show a constant presence of numerous xenomorphic inclusions and fractures. The crystals are not clear, displaying corroded terminations frequently and, sometimes, evident corrosion gulfs, whereas crystals with rims of metamorphic overgrowth were not observed.

The analyses shown in Table 2 and Figure 13A are generally discordant while only 3 of the 25 zircons have

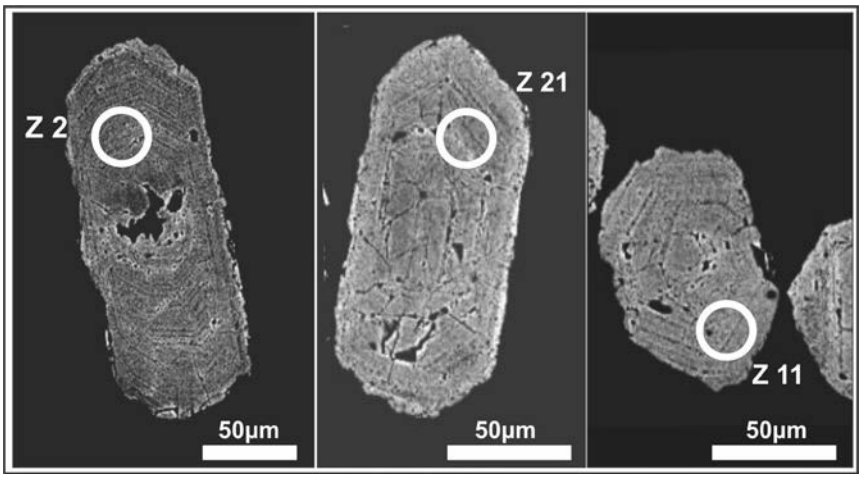

FIGURE 12 - Backscattered electron images of representative augen gneiss zircons, emphasizing growth zonation, xenomorphic inclusions, fractures and corroded rims (sample AR-44C).

TABLE 2 - U-Pb zircon isotopic data of the augen gneiss from the Saquinho stratigraphic hole (FD-SE-002). Sample AR-44C, 733.005 mE; 9.306.051 mN UTM coordinates (WGS84 Datum, Zone 24), depth = 121.0 to 122.0 m.

Spot grain	f206(%)	Th/U	$^{206}Pb/^{204}Pb$	$^{207}Pb/^{206}Pb$	err (%) 1σ.	$^{207}Pb/^{235}U$ (Ma)	err (%) 1σ.	$^{206}Pb/^{238}U$	err (%) 1σ.	Rho	$^{207}Pb/^{206}Pb$ (Ma)	$^{207}Pb/^{235}U$ (Ma)	$^{207}Pb/^{238}U$ (Ma)	Conc. (%)
004-Z1	0.35	0.52	4650	0.122817	0.21	4.067	2.32	0.240187	2.31	1.00	1998 ± 4	1648 ± 19	1388 ± 29	84.21
005-Z2	0.76	0.37	2233	0.107154	0.18	2.620	1.00	0.177332	0.99	0.98	1752 ± 3	1306 ± 7	1052 ± 10	80.56
006-Z3	0.40	0.41	4226	0.103501	0.57	2.617	2.23	0.183370	2.15	0.97	1688 ± 11	1305 ± 16	1085 ± 21	83.15
013-Z4	0.01	0.46	262149	0.128244	0.50	3.934	2.05	0.222509	1.99	0.97	2074 ± 9	1621 ± 17	1295 ± 23	79.91
014-Z5	0.01	0.61	117351	0.137087	0.27	7.021	0.83	0.371448	0.78	0.94	2191 ± 5	2114 ± 7	2036 ± 14	96.32
015-Z6	0.00	0.33	419023	0.130814	0.34	5.457	2.79	0.302569	2.77	0.99	2109 ± 6	1894 ± 24	1704 ± 41	89.97
016-Z7	0.00	0.51	301259	0.138668	0.31	7.837	1.07	0.409890	1.02	0.95	2211 ± 5	2212 ± 10	2214 ± 19	100.09
023-Z8	0.01	0.39	203772	0.133803	0.23	5.611	1.43	0.304145	1.41	0.99	2148 ± 4	1918 ± 12	1712 ± 21	89.26
024-Z9	0.01	0.50	147927	0.136797	0.21	6.987	0.80	0.370455	0.77	0.96	2187 ± 4	2110 ± 7	2032 ± 13	96.29
025-Z10	0.01	0.37	123331	0.128906	0.16	4.749	0.87	0.267170	0.86	0.98	2083 ± 3	1776 ± 7	1526 ± 12	85.95
026-Z11	0.56	0.45	2963	0.114918	0.23	3.353	0.74	0.211632	0.70	0.95	1879 ± 4	1494 ± 6	1238 ± 8	82.86
034-Z12	0.01	0.41	188228	0.132078	0.23	5.397	0.67	0.296369	0.63	0.92	2126 ± 4	1884 ± 6	1673 ± 9	88.80
035-Z13	0.05	0.30	37804	0.091437	0.72	1.939	1.70	0.153771	1.54	0.90	1456 ± 14	1095 ± 11	922 ± 13	84.24
036-Z14	0.20	0.46	8164	0.121775	0.31	3.917	0.98	0.233300	0.93	0.95	1982 ± 5	1617 ± 8	1352 ± 11	83.59
043-Z15	0.24	0.25	7139	0.081685	0.25	1.488	1.67	0.132104	1.65	0.99	1238 ± 5	925 ± 10	800 ± 12	86.43
044-Z16	0.07	0.41	22458	0.116407	0.31	3.382	1.30	0.210692	1.27	0.97	1902 ± 6	1500 ± 10	1233 ± 14	82.16
045-Z17	0.02	0.46	99950	0.125275	0.30	4.700	1.63	0.272076	1.60	0.98	2033 ± 5	1767 ± 14	1551 ± 22	87.79
046-Z18	0.18	0.37	9680	0.096158	0.46	2.061	2.16	0.155469	2.11	0.98	1551 ± 9	1136 ± 15	932 ± 18	82.00
053-Z19	0.60	0.54	2824	0.103044	0.46	2.458	1.46	0.173014	1.39	0.95	1680 ± 8	1260 ± 10	1029 ± 13	81.65
054-Z20	0.03	0.77	56182	0.127507	0.39	5.036	1.09	0.286443	1.02	0.93	2064 ± 7	1825 ± 9	1624 ± 15	88.95
055-Z21	0.03	0.73	57694	0.085668	0.52	1.411	1.40	0.119487	1.30	0.92	1331 ± 10	894 ± 8	728 ± 9	81.41
056-Z22	0.14	0.50	12654	0.110765	0.86	2.475	2.41	0.162069	2.25	0.93	1812 ± 16	1265 ± 17	968 ± 20	76.55
064-Z23	0.07	0.44	25708	0.102698	0.52	2.483	1.73	0.175354	1.65	0.95	1673 ± 10	1267 ± 13	1042 ± 16	82.20
065-Z24	0.05	0.29	33920	0.084780	0.40	1.511	1.30	0.129272	1.24	0.95	1311 ± 8	935 ± 8	784 ± 9	83.83
066-Z25	0.03	0.29	52123	0.101436	0.56	2.423	1.32	0.173229	1.19	0.90	1651 ± 10	1249 ± 9	1030 ± 11	82.43

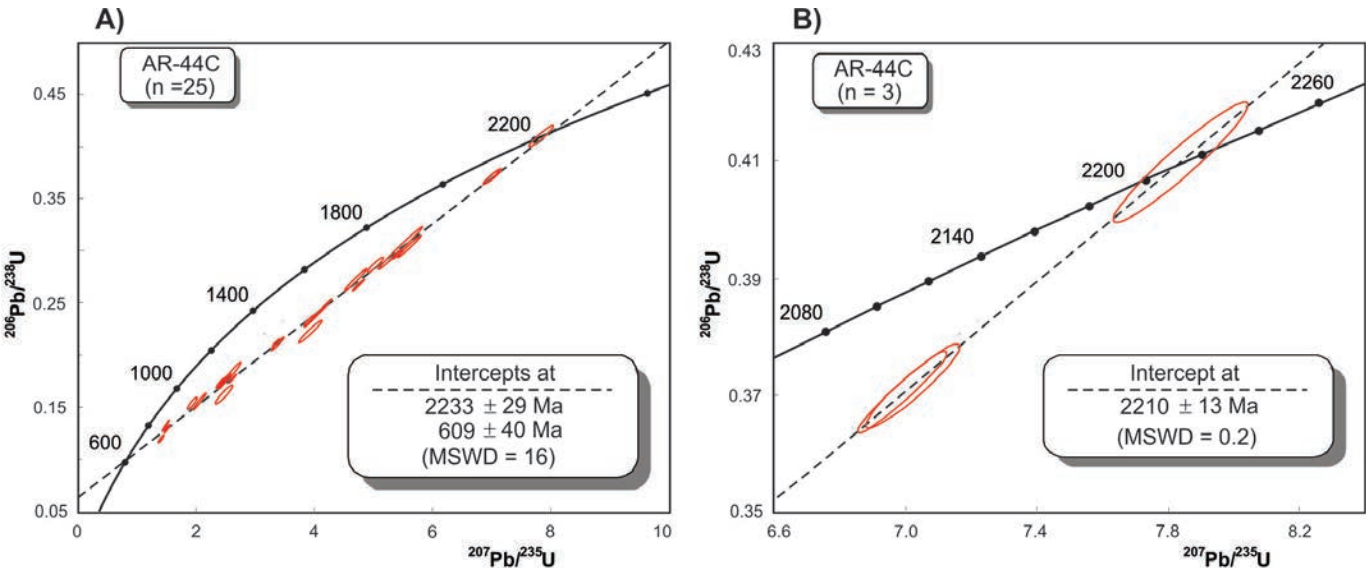

FIGURE 13 - Concordia diagrams for augen gneiss zircons between 121 and 122 m deep.

discordance <5%. The $^{206}Pb/^{204}Pb$ ratio also varied greatly, suggesting possible continuous losses of Pb and apparent ages of 700 to 2000 Ma. These varied analytical results obtained for the same rock possibly resulted from the previously mentioned frequent fractures observed in these non-clear and corroded zircons and/or the effect of a metamorphic event (Ediacaran?).

The data define a discordance with upper and lower intercepts of 2233 ± 29 Ma and 609 ± 40 Ma, respectively (MSWD = 16, Fig. 13A). Furthermore, the age calculated for the three zircons with concordance > 95% (Table 2, Z5-Z7-Z9) near the upper intercept (Fig. 13B), provide an average of 2210 ± 13 Ma (MSWD = 0.2), which overlaps the age obtained with all crystals, within the uncertainty limits.

This Rhyacian age (2210 ± 13 Ma) is considered the best approximation to the crystallization age of the augen gneiss protolith of the Saquinho hole, in agreement with the U-Pb zircon age (2171 ± 20 Ma) obtained for similar lithotypes in the Genezaré/Caicó region by Medeiros et al. (2012b), and other augen gneiss bodies in the Rio Piranhas-Seridó Domain by Hollanda et al. (2011). Souza et al. (2016) also obtained Rhyacian ages for orthogneisses from the Caicó region.

The Ediacaran age (ca. 609 Ma) of the discordant lower intercept (Fig. 13A) could possibly reflect the action of the Brasiliano Orogenesis. However, the texture analysis of the zircons showed no evidence of neoformed zircons or overgrowth textures and/or rims of metamorphic recrystallization. Even so, Pb loss due to orogeny may be the cause for that age.

4.5.2. Micro*augen* gneiss

A sample of amphibole-biotite microaugen gneiss (AR-62C), of monzogranitic composition and grayish color, was collected between 210.3 and 211.3 meters deep (Fig. 5). The zircons are predominantly prismatic, sometimes bipyramidal, with well-preserved faces, although some crystals have corroded rims. They are well developed, between 350 and 500 µm long whereas the small ones are 150-200 µm long (length/width = 3.1 to 3.9). Although there are few fractured crystals with, sometimes, filled fractures and ellipsoidal quartz inclusions, most zircon crystals are clear, with simple, homogeneous structures and some discrete growth zoning. Rarely, the crystals exhibited a thin rim that could eventually be attributed to metamorphic growth. The analysis points were generally positioned in clear locations in the crystal center, although the crystals were always homogeneous. Fig. 14 shows photos illustrating the types of crystals analyzed.

The analytical results in Table 3 do not show significant differences in the isotopic ratios and apparent ages between major and minor zircons. All points are concordant or less than 2% discordant, and yielded a concordant age of 2512 ± 3.2 Ma (Fig. 15). The zircon textures and the Th/U ratio between 0.13 and 0.65 are compatible with magmatic rocks (Beluosova et al. 2002; Hoskin and Schaltegger 2003), allowing to interpret this age as the crystallization time of the protolith of this microaugen gneiss, indicating the end of Neoarchean as the crystallization age of this unit.

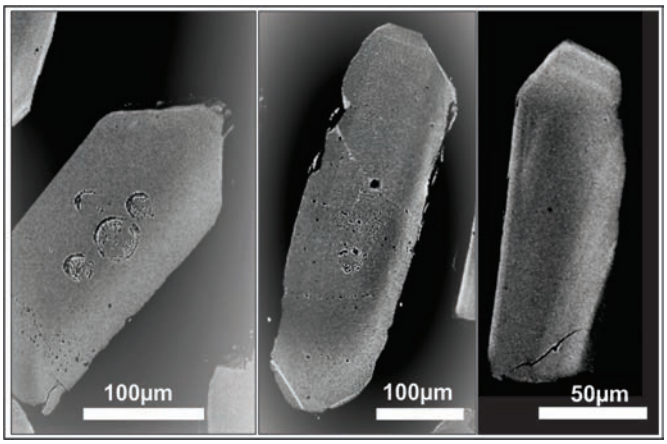

FIGURE 14 - Backscattered electron images of microaugen gneiss zircons emphasizing well-developed and prismatic shapes, clear crystals without metamorphic overgrowth rims (sample AR-62C).

TABLE 3 - U-Pb zircon isotopic data of the microaugen gneiss of the Saquinho stratigraphic hole (FD-SE-002). Sample AR-62C, 733.005 mE; 9.306.051 mN UTM coordinates (Datum WGS84, Zone 24), depth = 210.30 at 211.30 m.

Spot grain	f206(%)	Th/U	$^{206}Pb/^{204}Pb$	$^{207}Pb/^{206}Pb$	err (%) 1σ	$^{207}Pb/^{235}U$	err (%) 1σ.	$^{206}Pb/^{238}U$	err (%) 1σ.	Rho	$^{207}Pb/^{206}Pb$ (Ma)	$^{207}Pb/^{235}Pb$ (Ma)	$^{206}Pb/^{238}Pb$ (Ma)	Conc. (%)
ZR53	0.04	0.240	35640	0.16131	0.86	10.453	1.78	0.4700	1.51	0.85	2469 ± 29	2483 ± 62	2476 ± 33	100.56
ZR07	0.02	0.534	63346	0.16391	0.96	10.585	1.39	0.4684	0.94	0.68	2496 ± 32	2476 ± 39	2487 ± 26	99.20
ZR44	0.01	0.164	240999	0.16265	0.80	10.664	1.67	0.4755	1.42	0.85	2483 ± 27	2508 ± 59	2494 ± 31	100.97
ZR05	0.02	0.454	64768	0.16503	0.91	10.726	1.45	0.4714	1.07	0.74	2508 ± 30	2490 ± 44	2500 ± 27	99.27
ZR54	0.01	0.224	137607	0.16599	0.82	10.752	1.77	0.4698	1.52	0.86	2518 ± 28	2482 ± 63	2502 ± 33	98.61
ZR01	0.03	0.345	50176	0.16533	0.81	10.752	1.26	0.4716	0.90	0.71	2511 ± 27	2491 ± 37	2502 ± 23	99.20
ZR04	0.02	0.456	83372	0.16520	0.73	10.753	1.14	0.4720	0.80	0.70	2510 ± 24	2492 ± 33	2502 ± 21	99.31
ZR06	0.02	0.281	74669	0.16624	0.99	10.784	1.52	0.4705	1.10	0.72	2520 ± 33	2486 ± 45	2505 ± 28	98.63
ZR12	0.12	0.336	12515	0.16582	1.09	10.853	1.66	0.4746	1.19	0.72	2516 ± 36	2504 ± 49	2511 ± 31	99.52
ZR08	0.10	0.365	14620	0.16345	1.40	10.872	2.01	0.4824	1.39	0.69	2492 ± 47	2538 ± 58	2512 ± 37	101.85
ZR20	0.04	0.396	36620	0.16555	0.73	10.874	1.24	0.4763	0.93	0.75	2513 ± 24	2511 ± 39	2512 ± 23	99.92
ZR16	0.04	0.449	39398	0.16660	0.97	10.882	1.64	0.4737	1.26	0.77	2524 ± 32	2500 ± 52	2513 ± 30	99.05
ZR13	0.34	0.315	4334	0.16419	2.15	10.883	3.12	0.4807	2.24	0.72	2499 ± 71	2530 ± 93	2513 ± 57	101.24
ZR34	0.01	0.570	185421	0.16585	0.80	10.895	1.26	0.4764	0.89	0.71	2516 ± 27	2512 ± 37	2514 ± 23	99.82
ZR10	0.03	0.413	52753	0.16616	0.72	10.952	1.33	0.4780	1.06	0.79	2519 ± 24	2519 ± 44	2519 ± 25	99.97
ZR56	0.01	0.129	149212	0.16627	0.77	10.953	1.22	0.4777	0.87	0.71	2520 ± 26	2517 ± 36	2519 ± 23	99.88
ZR49	0.01	0.391	146706	0.16417	0.80	10.969	1.49	0.4845	1.21	0.81	2499 ± 27	2547 ± 51	2521 ± 28	101.92
ZR58	0.01	0.584	147503	0.16595	1.09	10.972	1.51	0.4795	0.97	0.65	2517 ± 36	2525 ± 41	2521 ± 28	100.31
ZR30	0.01	0.254	184874	0.16688	0.71	11.007	1.70	0.4783	1.50	0.88	2527 ± 24	2520 ± 63	2524 ± 31	99.74
ZR23	0.02	0.352	62254	0.16729	1.16	11.035	1.74	0.4784	1.24	0.71	2531 ± 39	2520 ± 52	2526 ± 32	99.58
ZR11	0.15	0.445	9804	0.16740	2.04	11.072	3.59	0.4796	2.93	0.82	2532 ± 68	2526 ± 122	2529 ± 66	99.76
ZR55	0.01	0.476	162281	0.16648	0.88	11.105	1.45	0.4837	1.09	0.75	2523 ± 29	2544 ± 46	2532 ± 27	100.83
ZR37	0.00	0.650	419431	0.16734	0.90	11.147	1.36	0.4831	0.95	0.70	2531 ± 30	2541 ± 40	2536 ± 25	100.38
ZR32	0.00	0.472	530254	0.16577	0.57	11.154	1.14	0.4880	0.91	0.80	2515 ± 19	2562 ± 38	2536 ± 21	101.85

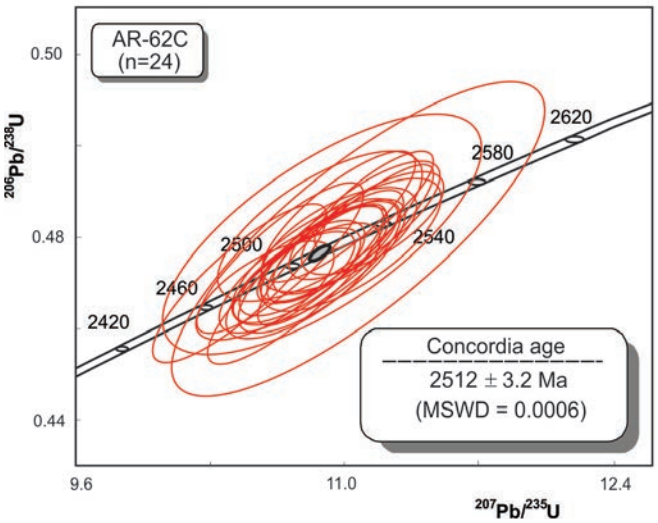

FIGURE 15 - Concordia diagram for zircons of the microaugen gneiss (sample AR-62C) between 210.3 and 211.3m deep.

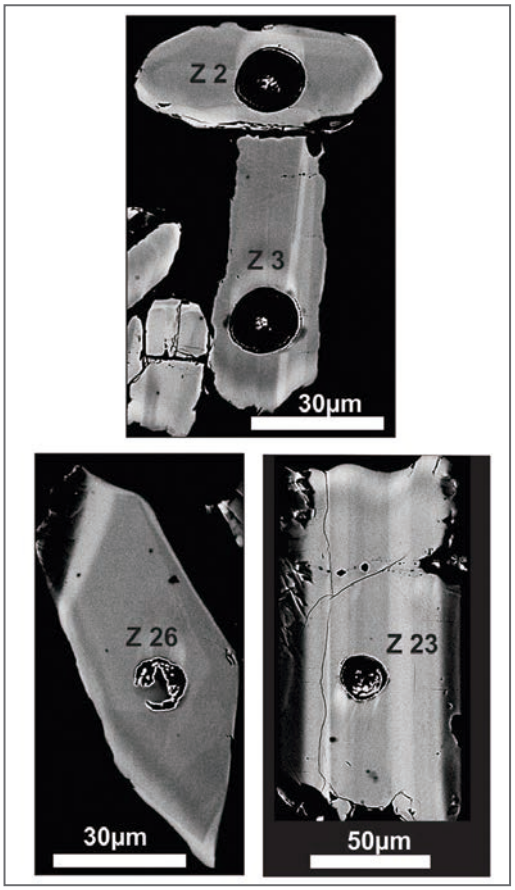

FIGURE 16 - Backscattered electron images representing the metagabbronorite zircons, exhibiting crystals with sinuous edges and often with corrosion gulfs (sample AR-75C).

4.5.3. Metagabbronorite

A metagabbronorite sample from the metamafic sequence of the lower compartment (AR-75C) was obtained between 331.15 and 332.05 m deep (Fig. 5). The zircons are generally short prismatic with length to width ratio seldom exceeding 2. In general, the crystals are between 50 and 150 µm long, have almost always corroded and irregular rims, many shaped like gulfs, with broken and jagged frontal endings (Fig. 16). There are inclusions of small circular and, sometimes, aligned minerals whose crystals often exhibit discontinuous, sinuous fractures. However, these crystals do not have complex textures, being homogeneous and limpid with discrete growth zonation, when present. Rarely, the crystals show a probable rim of metamorphic overgrowth, but the analyses were performed in the crystals center to avoid the fractures.

The data in Table 4 show that the great majority of the crystals plot on or very close to the concordia, with <2% discordance, and rare points a little more discordant. The high values of the $^{206}Pb/^{204}Pb$ ratio indicate the excellent quality of the obtained values while the Th/U ratios up to 0.6 are compatible with those of igneous zircons (Beluosova et al. 2002; Hoskin and Schaltegger 2003). Together, the points produce an excellent alignment (Fig. 17) defining an age of 2501 ± 2.7 Ma, interpreted as the crystallization age of the rock protolith at the end of Neoarchean.

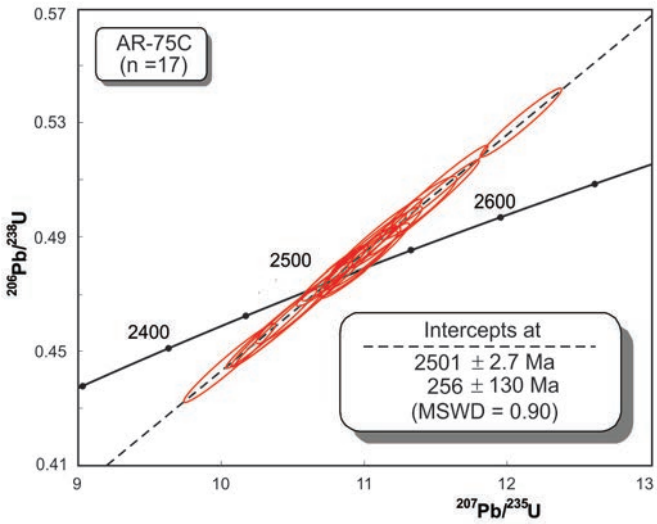

FIGURE 17 - Concordia diagram for metagabbronorite zircons between 331.15 and 332.05 m deep (sample AR-75C).

TABLE 4 - U-Pb zircon isotopic data for the metagabbronorite from the Saquinho stratigraphic borehole (FD-SE-002). Sample AR-75C, 733.005 mE; 9306.051 mN UTM coordinates (WGS84 Datum, Zone 24), depth = 331.15 to 332.05 m.

Spot grain	f206(%)	Th/U	$^{206}Pb/^{204}Pb$	$^{207}Pb/^{206}Pb$	err (%) 1σ.	$^{207}Pb/^{235}U$	err (%) 1σ.	$^{206}Pb/^{238}U$	err (%)1σ.	Rho	$^{207}Pb/^{206}Pb$ (Ma)	$^{207}Pb/^{235}U$ (Ma)	$^{206}Pb/^{238}U$ (Ma)	Conc. (%)
004-Z1	0.01	0.25	246929	0.164534	0.26	10.658	2.14	0.469792	2.12	0.99	2503 ± 4	2494 ± 20	2483 ± 44	99.20
006-Z3	0.01	0.47	248365	0.164266	0.23	11.000	1.07	0.485664	1.04	0.98	2500 ± 4	2523 ± 10	2552 ± 22	102.07
008-Z5	0.01	0.57	180352	0.164009	0.26	10.760	0.90	0.475821	0.86	0.95	2497 ± 4	2503 ± 8	2509 ± 18	100.47
009-Z6	0.01	0.40	164884	0.164935	0.33	11.371	0.96	0.500014	0.91	0.93	2507 ± 6	2554 ± 9	2614 ± 19	104.27
013-Z8	0.00	0.65	433908	0.165002	0.34	10.981	0.99	0.482691	0.93	0.93	2508 ± 6	2522 ± 9	2539 ± 20	101.25
014-Z9	0.01	0.38	255828	0.163553	0.30	10.057	1.30	0.445963	1.27	0.97	2493 ± 5	2440 ± 12	2377 ± 25	95.37
016-Z11	0.02	0.40	92197	0.164213	0.29	10.480	0.94	0.462864	0.89	0.95	2500 ± 5	2478 ± 9	2452 ± 18	98.11
018-Z13	0.01	0.51	138640	0.163893	0.23	10.348	1.26	0.457907	1.23	0.98	2496 ± 4	2466 ± 12	2430 ± 25	97.36
019-Z14	0.01	0.39	152709	0.164625	0.24	11.516	1.21	0.507342	1.18	0.98	2504 ± 4	2566 ± 11	2645 ± 26	105.65
024-Z16	0.01	0.39	123383	0.164127	0.28	11.069	1.21	0.489128	1.18	0.97	2499 ± 5	2529 ± 11	2567 ± 25	102.73
029-Z21	0.01	0.60	100822	0.165403	0.23	12.088	0.96	0.530025	0.93	0.97	2512 ± 4	2611 ± 9	2742 ± 21	109.15
030-Z22	0.01	0.43	132947	0.164964	0.29	11.140	0.95	0.489783	0.90	0.95	2507 ± 5	2535 ± 9	2570 ± 19	102.49
034-Z23	0.01	0.51	181036	0.165402	0.26	11.406	1.40	0.500140	1.37	0.98	2512 ± 4	2557 ± 13	2614 ± 29	104.09
036-Z25	0.01	0.22	133376	0.164338	0.30	10.490	1.65	0.462948	1.62	0.98	2501 ± 5	2479 ± 15	2453 ± 33	98.07
037-Z26	0.01	0.48	170820	0.165593	0.30	10.999	1.15	0.481739	1.11	0.96	2514 ± 5	2523 ± 11	2535 ± 23	100.85
038-Z27	0.02	0.13	85898	0.163921	0.25	10.792	0.87	0.477473	0.83	0.95	2497 ± 4	2505 ± 8	2516 ± 17	100.79
040-Z29	0.01	0.58	138585	0.165237	0.33	10.954	1.02	0.480792	0.96	0.94	2510 ± 6	2519 ± 9	2531 ± 20	100.83

5. Geological model

A geological model using the surface mapping data in semi-detail and detail scales, mining pits mapping, Saquinho stratigraphic hole (FD-SE -002) and drill holes provided by Susa Indústria e Comércio de Productos Minerários Ltd is here proposed to understand better the geodynamic events in the region of the Saquinho iron deposit. The vertical geological section (Fig. 18) shows, at the top, a rock sequence of the Jucurutu Formation represented by biotite paragneiss, amphibole-biotite schist, marble, garnet amphibolite and banded iron formation. Below the Jucurutu Formation, a biotite augen gneiss with amphibole was observed, whose contact with the upper strata occurs due to nonconformity, and, in some places, through shear zones. The basal contact between the augen gneiss and the underlying Archean unit was considered intrusive.

These lithological contents and the obtained Neoarchean age, previously unknown for the Rio Piranhas-Seridó Domain, allows suggesting the term Saquinho Complex for this unit. The site of the FD-SE-002 hole at depth of 165 to 440m is taken as the region of its stratotype.

In this context, a geological model is proposed for the region of the Saquinho iron mine, from a substrate with age of the end of the Neoarchean. Subsequently, this substrate was intruded by a porphyritic granitoid (protolith of the Rhyacian augen gneiss) representing the intermediate compartment. A weathering/erosion process followed, with subsidence at least partially favored by the action of normal faults (?) and beginning of sediment deposition of what would become the Saquinho Basin (upper compartment). This compartment is represented by the metasediments of the Jucurutu Formation (Ediacaran), with the banded iron formation developing at the base of the sequence. In the final installation phase, the basin is affected by the Brasiliano orogenesis, when folds and reactivations of the normal faults occurred, determining the final structuring of the basin (Figure 19).

The participation of mafic rocks such as those observed in the lower compartment in the iron mineralization process is commonly reported in the literature (Lindenmayer et al. 2002; Lobato et al., 2005; Rosière et al., 2006; Zuchetti 2007). In the genesis of the iron formations, the iron source would be related to two possibilities: (i) leaching of iron-rich lithologies (e.g., mafic/ultramafic rocks); (ii) introduced by subaquatic

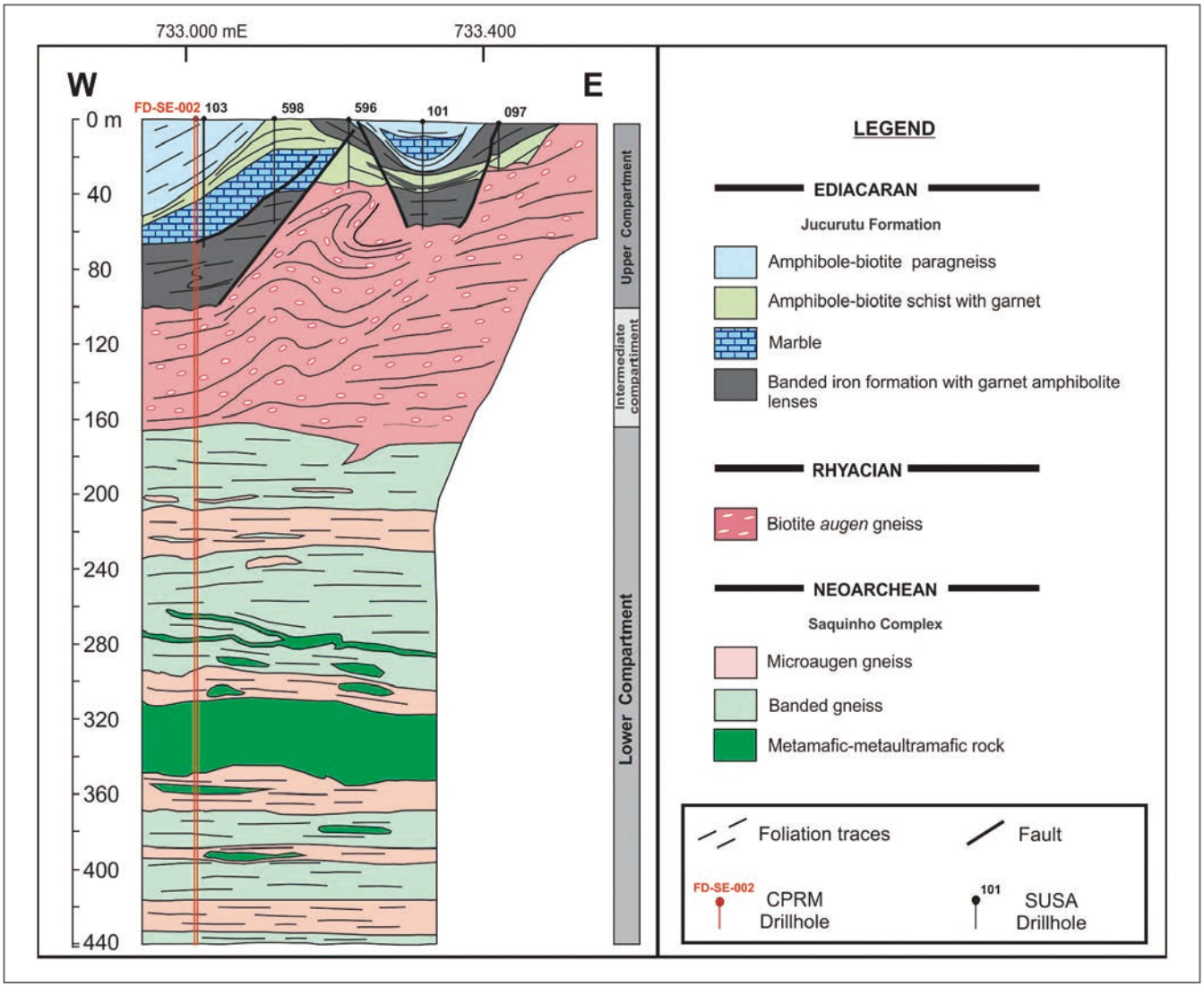

FIGURE 18 - Geological section of northern Saquinho iron mine, composed of the FD-SE-002 borehole and others made by Susa Indústria e Comércio de Produtos Minerários Ltd.

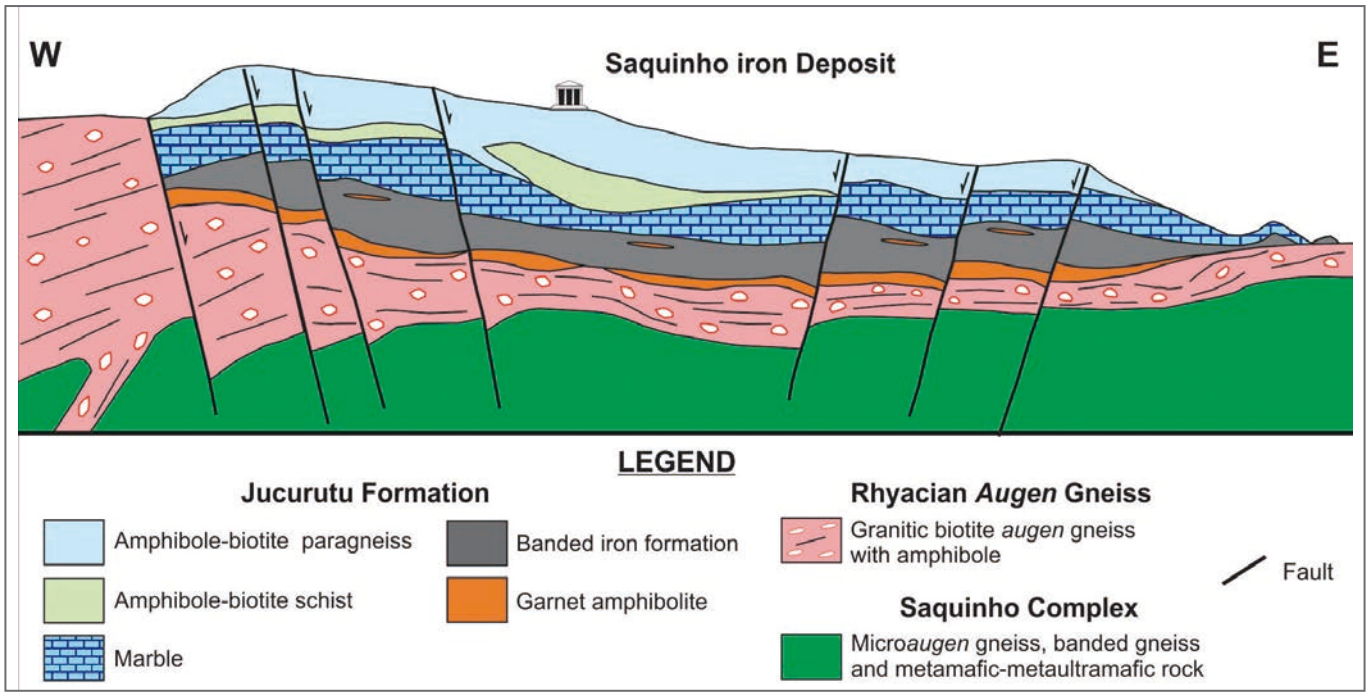

FIGURE 19 - Geological model of the Saquinho mine region (without scale), emphasizing the metasediments of the Jucurutu Formation superimposed on a basement composed of Rhyacian and Archean rocks.

hydrothermal discharges into lake environments and ocean basins. For both hypotheses to be plausible, a stratified density system must act, that is, currents need to transport the reduced iron from deeper anoxic waters to a shallow water oxygenated environment where Fe^{2+} is oxidized and precipitated as oxides and carbonates.

Currently, several authors (Klein and Beukes 1989; Klein 2005; Pirajno 2009) agree that iron was introduced into the ocean from hydrothermal vents, followed by the deposition of iron formations on the continental shelf and upper slope, in a layer of oxide-anoxic stratified water.

The proposed origin for the iron formations in the Saquinho area would be related to the interaction of hydrothermal fluids with the Neoarchean mafic rocks previously emplaced in the floor of this basin, which acted as leachers, removing (mainly) elements such as iron and magnesium and enriching the paleobasin. In addition, we speculate the presence of vents that would be responsible for the hydrothermal iron discharges in the basins.

The stratigraphic study based on the $\delta^{13}C$ and $\delta^{18}O$ isotopic data of the Saquinho marbles show compositions with a broad spectrum signature represented by the $\delta^{13}C$ (2.4 and 10.4‰) and $\delta^{18}O$ (-9.7 and -5.3‰) values, which can be interpreted as a carbon source derived from marine carbonate rocks (Nascimento et al. 2004, 2007; Sial et al. 2015; Campos 2011).

6. Conclusions

The age of 2210 ± 13 Ma obtained for the augen gneiss of syenogranite to alkali feldspar granite, from 107.9 to 165.1 m deep, is similar to those mapped and dated in adjacent regions, indicating a Rhyacian age for this rock.

The ages of 2512 and 2501 Ma (end of Neoarchean) obtained for the rocks of the units placed below the augen gneisses (lower compartment of the stratigraphic hole) indicate a unit distinct from those previously mentioned in the Rio Piranhas-Seridó Domain, which we name here as the Saquinho Complex.

The presence of metamafic-metaultramafic rocks with disseminated sulfide (pyrite, chalcopyrite, and pyrrhotite), even in the small amount observed, allow considering these rocks as a new geological/metallogenic potential for the region.

The marbles in the Saquinho hole occur between 46.7 and 66.3 m deep, presenting petrographic, stratigraphic and isotopic compositions ($\delta^{13}C$ and $\delta^{18}O$) similar to those described in the literature for the Jucurutu Formation, but distinct from those of the Seridó Formation and those considered as of older/Archean ages. The carbon and oxygen isotopic data show values that corroborate the models proposed in the literature, which interpreted as from a source derived from marine carbonate rocks.

The geological model of the Saquinho Basin is divided into three large compartments, with the installation of brittle and/or ductile/brittle structures with successive reactivations that probably acted as conduits for percolation of fluids that generated the ferriferous formations.

Acknowledgments

The authors thank the CPRM- Geological Survey of Brazil for providing the data, the Department of Geology of the Universidade Federal do Rio Grande do Norte and the Laboratory of Stable Isotopes of the Universidade de Brasília, for the support preparing the samples and acquiring the analytical results. Thanks are also due to Susa Indústria e Comércio de Produtos Minerários Ltd for allowing access to the area, the boreholes, as well as to the reviewers, Sérgio Pacheco Neves and Zorano Sérgio de Souza, for the suggestions that contributed to improving this manuscript.

References

Almeida F.F.M., Hasui Y., Brito Neves B.B., Fuck R. 1981. Brazilian structural provinces: an introduction. Earth-Science Reviews, 17, 1-29.

Belousova E.A., Griffin W.L., O´Reilly S.Y., Fisher N.I. 2002. Igneous zircon: trace element composition as an indicator of source rock type. Contribution Mineralogy Petrology, 143, 602-622. DOI 10.1007/s00410-002-0364.7.

Beukes J.B., Gutzmer J. 2008. Origin and paleoenvironmental significance of major iron formations at the Archean-Paleoproterozoic boundary: Reviews. Economic Geology, 15, 5-48.

Beurlen H. 1995. The mineral resources of the Borborema Province in the Northeastern of Brazil and its sedimentary cover: a review. Journal of South American Earth Sciences, 8, 365-376.

Biondi J.C. 2003. Processos metalogenéticos e os depósitos minerais brasileiros. São Paulo, Oficina de Textos –CBMM, 528p.

Brito Neves B.B., Santos E.J., Van Schmus W.R. 2000. Tectonic history of the Borborema province, northeastern Brazil. In: International Geological Congress, 31, 151-182.

Bühn B., Pimentel M.M., Matteini M., Dantas E.L. 2009. High spatial resolution analysis of Pb and U isotopes for geochronology by lases ablation multi-collector inductively coupled plasma mass spectrometry (LA-MC-IC-MS). Anais da Academia Brasileira de Ciências, 81, 99-114.

Campos M.S. 2011. Quimioestratigrafia isotópica de carbono e estrôncio e geoquímica de elementos terras raras em formações carbonáticas e ferríferas do Cinturão Seridó, Nordeste do Brasil. MSc Dissertation, Programa de Pós-Graduação em Geociências, Universidade Federal de Pernambuco, Recife, 99 p.

Cavalcante R., Cunha A.L.C., Medeiros V.C. 2015. Mapa geológico do Projeto Províncias Metalogenéticas do Brasil: área PB - RN (Borborema Leste), escala 1:250.000. Programa Geologia do Brasil. Recife, CPRM. Available at: <http://geosgb.cprm.gov.br> (access in January 2018).

Cavalcante R., Cunha A.L.C., Oliveira R.G., Medeiros V.C., Dantas A.R., Costa A. P., Lins C.A.C., Larizzatti J.H. 2016. Metalogenia das Províncias Minerais do Brasil: área Seridó leste, extremo NE da Província Borborema (RN-PB). Série Províncias Minerais do Brasil, 8. Brasília, CPRM, 103 p. Available at: <http://www.cprm.gov.br>.

Costa A.P., Dantas A.R. 2014. Carta Geológica da Folha Lajes SB.24-X-D-VI, Estado do Rio Grande do Norte, Escala 1:100.000. Programa Geologia do Brasil. Recife, CPRM. Available at: <http://geosgb.cprm.gov.br> (access in January 2018).

Costa A.P., Dantas A.R., Dreher A.M., Benedictus A., Jaime P., Riffel S.B. 2014. Petrographic characterization with Qemscan Analysis of Fe-Ti occurrence associated with ultramafic rocks in São Tomé (RN), Brazil. In: Simpósio Brasileiro de Exploração Mineral - Simexmin, 6. Avaliable at: < http://www.adimb.com.br/simexmin2014> (access in January 2018).

Dantas A.R., Nascimento M.A.L., Costa A.P., Cavalcante R. 2017. Petrografia e litoquímica de rochas ferríferas na região central do estado do Rio Grande do Norte (Domínio Rio Piranhas - Seridó, NE da Província Borborema). Geologia USP, Série Científica, 17(3), 163-187.

Dantas E.L. 1988. Mapeamento geológico da região de Florânia-RN. Graduation work, Departamento de Geologia, Universidade Federal do Rio Grande do Norte, Natal, 270 p.

Dantas E.L. 1992. Evolução tectono-magmática do maciço polidiapírico São Vicente/Florânia-RN. MSc Dissertation, Instituto de Geociências e Ciências Exatas, Universidade Estadual Paulista, Rio Claro, 272 p.

Dantas E.L. 1996. Geocronologia U-Pb e Sm-Nd de terrenos arqueanos e paleoproterozoicos do maciço Caldas Brandao, NE Brasil. Ph.D. Thesis, Instituto de Geociências e Ciências Exatas, Universidade Estadual Paulista, Rio Claro, 206 p.

Dantas E.L., Roig H.L. 2013. Carta Geológica da Folha São José do Campeste SB.25-Y-A-I, Estados do Rio Grande do Norte e da Paraíba, Escala 1:100.000. Brasília, CPRM. Available at: <http://geosgb.cprm.gov.br> (access in January 2018).

Dantas E.L., Hackspacher P.C., Van Schmus W.R., Neves B.B.B. 1997. Archean accretion in the Caldas Brandão Massif, Borborema Province, Northeast Brazil. Revista Brasileira de Geociências, 28, 221-228.

Dantas E.L., Van Schmus W.R., Hackspacher P.C., Fetter A.H., Brito Neves B.B., Cordani U.G., Nutman A.P., Williams I.S. 2004. The 3.4-3.5 Ga São José do Campestre massif, NE Brazil: remnants of the oldest crust in South America. Precambrian Research, 130, 113-137.

Dantas E.L., Souza Z.S., Wernick E., Hackspacher P.C., Xiaodong D., Li, J.W. 2013. Crustal growth in the 3,4-2,7Ga São José de Campestre Massif, Borborema Province, NE Brazil. Precambrian Research, 227, 120-156.

Dantas R.C., Dantas E.L., Oliveira, C.G. 2014. Geoquímica e geocronologia U-Pb e Sm-Nd das rochas encaixantes arqueanas do depósito de W-Au Bonfim-RN, Faixa Seridó, Província Borborema. In: Congresso Brasileiro de Geologia, 47, 1914. CD-ROOM.

Ebert H. 1969. Geologia do Alto Seridó: nota explicativa da folha geológica de Currais Novos. Série Geologia Regional, 11. Recife, SUDENE, 120p.

Ferreira C.A. 1998. Caicó (SB.24-Z-B), escala 1:250.000, estados do Rio Grande do Norte e da Paraíba. Brasília, CPRM, 152 p.

Figueiredo B.S. 2012. Geoquímica e gênese das formações ferríferas e metacarbonatos da porção sul do maciço São José do Campestre, Província Borborema. MSc Dissertation, Universidade de Brasília, Brasília, 108 p.

Hackspacher P.C., Van Schmus W.R., Dantas E.L. 1990. Um embasamento transamazônico na Província Borborema. In: Congresso Brasileiro de Geologia, 36, 2683-2696.

Hollanda M.H.B.M., Archanjo J.C., Souza L.C., Dunyi L., Armstrong R. 2011. Long-lived Paleoproterozoic granitic magmatism in the Seridó-Jaguaribe domain, Borborema Province–NE Brazil. Journal of South American Earth Sciences, 32, 287-300.

Hollanda M.H.B.M., Archanjo C.J., Bautista J.R., Souza L.C. 2015. Detrital zircon ages and Nd isotope compositions of the Seridó and Lavras da Mangabeira basins (Borborema Province, NE Brazil): evidence for exhumation and recycling associated with a major shift in sedimentary provenance. Journal of South American Earth Sciences, 258, 186-207.

Hoskin P.W.O., Schaltegger U. 2003. The composition of zircon and igneous and metamorphic petrogenesis. Reviews in Mineralogy and Geochemistry, 53,27-62.

Jardim de Sá E.F. 1984. Geologia da região Seridó: reavaliação de dados. In: Simpósio de Geologia do Nordeste, 11, 278-296.

Jardim de Sá E.F. 1994. A Faixa Seridó (Província Borborema, NE do Brasil) e o seu significado geodinâmico na Cadeia Brasiliana/Pan-Africana. PhD Thesis, Universidade de Brasília, Brasília, 803 p.

Jardim de Sá E.F., Salim, J. 1980. Reavaliação dos conceitos estratigráficos na região do Seridó (RN-PB). Mineração e Metalurgia, 80, 16-28.

Jardim de Sá E.F., Legrand J.M., McReath I. 1981. “Estratigrafia” de rochas granitoides na região do Seridó (RN-PB) com base em critérios estruturais. Revista Brasileira de Geociências, 11, 50-57.

Jardim de Sá E.F., Macedo M.H.F., Fuck R.A., Kawashita K. 1992. Terrenos proterozóicos na Província Borborema e a margem norte do Cráton São Francisco. Revista Brasileira de Geociências, 22, 472-480.

Klein C. 2005. Some Precambrian banded iron-formations (BIFs) from around the world: Their age, geologic setting, mineralogy, metamorphism, geochemistry, and origins. American Mineralogist, 90, 1473-1499.

Klein C., Beukes N.J. 1989. Geochemistry and sedimentology of a facies transition from limestone to iron formation deposition in the Early Proterozoic Transvaal Supergroup, South Africa. Economic Geology, 84,1733-1774.

Legrand J.M, Liegeois J.P., Deutsch, S. 1991. Datação U/Pb e Rb/Sr das rochas precambrianas da região de Caicó. Reavaliação da definição de um embasamento arqueano. In: Simpósio de Geologia do Nordeste, 14, 276-279.

Lindenmayer Z.G., Laux J.H., Teixeira J.B.G., Fleck A., Galli C.P. 2002. Alteração hidrotermal das rochas intrusivas máficas do depósito de Cu-Au de Gameleira: uma comparação com a alteração das rochas intrusivas máficas da mina de Au do Igarapé Bahia e do depósito ferrífero de S11, Serra dos Carajás. In: Klein, E.L., Vasquez, M.L., Rosa-Costa, L.T. (eds.) Contribuições à geologia da Amazônia. Belém, SBG, p. 169-190.

Lobato L.M., Rosière C.A., Silva R.C.F., Zucchetti M., Baars F.J., Seoane J.C.S., Rios F.J., Pimentel M., Mendes G.E., Monteiro A.M. 2005. A mineralização hidrotermal de ferro da Província Mineral de Carajás: controle estrutural e contexto na evolução metalogenética da província. In: Marini O.J, Queiroz E.T de, Ramos B.W (eds.) Caracterização de depósitos minerais em distritos mineiros da Amazônia. Brasília, DNPM/CTMineral/FINEP/ADIMB, p. 25-92.

Ludwig K.R. 2003. User´s Manual fot Isoplot 3.00: a Geochronological Tollkit for Microsoft Excel. Berkeley Geochronology Center, Special Publication, 4, 74 p.

Maranhão R., Barreiro D.S., Silva A.P., Lima F., Pires P.R.R. 1986. A jazida de scheelita de Brejuí/Barra Verde/Boca de Lage/Zangarelhas, Rio Grande do Norte. In: Schobbenhaus C., Coelho C.E.S. (eds.) Principais depósitos minerais do Brasil. v. 2. Brasília, DNPM/CVRD/CPRM, p. 393-407.

Medeiros V.C., Dantas E.P. 2015. Geologia e recursos minerais da Folha Currais Novos, Estados do Rio Grande do Norte e da Paraíba. Recife, CPRM, 154p. Available at: <http://geosgb.cprm.gov.br> (access in January 2018).

Medeiros V.C., Nascimento M.A.L., Dantas E.L., Cunha A.L.C. 2012a. Carta Geológica da Folha Currais Novos SB.24-Z-B-II, Estados do Rio Grande do Norte e da Paraíba, Escala 1:100.000. Programa Geologia do Brasil. Recife, CPRM. Available at: <http://geosgb.cprm.gov.br> (access in January 2018).

Medeiros V.C., Nascimento M.A.L., Galindo A.C., Dantas E.L. 2012b. Augen gnaisses riacianos no Domínio Rio Piranhas-Seridó - Província Borborema, Nordeste do Brasil. Geologia USP, Série Científica, 12(2), 3-4.

Medeiros V.C, Cavalcante R., Cunha A.L.C., Dantas A.R., Costa A.P., Brito A.A., Rodrigues J.B., Silva M.A. 2017. O furo estratigráfico de Riacho Fechado (Currais Novos/RN), domínio Rio Piranhas-Seridó (província Borborema, NE Brasil): procedimentos e resultados. Estudos Geológicos, 27(3), 3-44.

Nascimento R.S.C., Sial A.N., Pimentel M.M. 2004. Chemostratigraphyc of medium-grade marbles of the late-Neoproterozoic Seridó Group, Seridó Fold Belt, northeastern Brazil. Gondwana Research, 7, 731-744.

Nascimento R.S.C., Sial A.N., Pimentel M.M. 2007. C- and Sr-isotope systematics applied to Neoproterozoic marbles of the Seridó belt, northeastern Brazil. Chemical Geology, 237, 191-210.

Nascimento M.A.L., Galindo A.C., Medeiros V.C. 2015. Ediacaran to Cambrian magmatic suites in the Rio Grande do Norte domain, extreme Northeastern Borborema Province (NE of Brazil): current knowledge. Journal of South American Earth Sciences, 58, 281-299.

Oliveira F.V. 2015. Chronus: um novo suplemento para a redução de dados U-Pb obtidos por LA-MC-ICPMS. MSc Dissertation, Universidade de Brasília, Brasília, 91 p.

Pessoa J. 1986. Mapeamento geológico estrutural de uma área a NW de Cruzeta. Graduation work, Departamento de Geologia, Universidade Federal do Rio Grande do Norte, Natal, 139 p.

Pirajno F. 2009. Hydrothermal processes and mineral systems. New York, Springer-Verlag, 1250 p.

Roig H.L., Dantas E.L. 2013. Carta Geológica da João Câmara SB.25-Y-A-IV, Estado do Rio Grande do Norte, Escala 1:100.000. Brasília, CPRM. Available at: <http://geosgb.cprm.gov.br> (access in January 2018).

Rosière C.A., Baars F.J., Seoane J.C.S., Lobato L.M., Silva L.L., Souza S.R.C., Mendes G.E. 2006. Structure and iron mineralisation of the Carajás Province. Applied Earth Science, 115, 126-133.

Ruiz F.V., Della Giustina M.E.S., Oliveira C.G., Dantas E.L., Hollanda M.H.B. 2018. The 3.5 Ga São Tomé layered mafic-ultramafic intrusion, NE Brazil: insights into a Paleoarchean Fe-Ti-V oxide mineralization and its reworking during West Gondwana assembly. Precambrian Research. Available at: <https://doi.org/10.1016/j.precamres.2018.03.011>

Salim J. 1979. Geologia e controles das mineralizações scheelitíferas da região da Serra do Feiticeiro e Bonfim, Lages, RN. MSc Dissertation, Universidade de Brasília, Brasília, 106 p.

Salim J. 1993. Géologie, pétrologie et géochimie des skarns à scheelite de la Mine Brejuí, Currais Novos, région du Seridó, NE du Brésil. PhD Thesis, Université Catholique de Louvain, Belgium, 272 p.

Santos E.J. 1996. Ensaio preliminar sobre terrenos e tectônica acrescionária na Província Borborema. In: Congresso Brasileiro de Geologia, 39, 47-50.

Santos E.J., Brito Neves B.B., Van Schmus W.R., Oliveira R.G., Medeiros V.C. 2000. An overall view on the displaced terrane arrangement of the Borborema Province, NE Brazil. In: International Geological Congress, 31, CD-ROM.

Sial A.N., Campos M.S., Gaucher C., Frei R., Ferreira V.P., Nascimento R.C., Pimentel M.M., Pereira N.S., Rodler A. 2015. Algoma-type Neoproterozoic BIF's and related marbles in the Seridó Belt (NE Brazil): REE, C, O, Cr and Sr isotope evidence. Journal of South American Earth Sciences, 61, 33-52.

Souza Z.S. 1991. Petrogénèse des metagranitoides du Complexe de Caicó, Province Borborema (Etat du Rio Grande do Norte, Brésil). MSc Dissertation, CAESS, Université de Rennes, Rennes, 87 p.

Souza Z.S., Martin H., Peucat J.-J., Jardim de Sá E.F., Macedo M.H.F. 2007. Calc-alkaline magmatism at the Archean and Proterozoic transition: the Caicó complex basement (NE Brazil). Journal of Petrology, 48, 2149-2185.

Souza Z.S., Kalsbeek F., Deng X-D., Frei R., Kokfelt T.F., Dantas E.L., Li J-W., Pimentel M.M., Galindo A.C. 2016. Generation of continental crust in the northern part of the Borborema Province, northeastern Brazil, from Archean to Neoproterozoic. Journal of South American Earth Sciences, 68, 68-96.

Souza Neto J.A., Legrand J.M., Volfinger M., Pascal M.L., Sonnet P. 2008. W–Au skarns in the Neo-Proterozoic Seridó Mobile Belt, Borborema Province in northeastern Brazil: an overview with emphasis on the Bonfim deposit. Mineralium Deposita, 43, 185-205.

Van Schmus W.R., Brito Neves B.B., Hackspacher P.C., Babinski M. 1995. U-Pb and Sm-Nd geochronologic studies of the Eastern Borborema Province, Northeast Brazil: initial conclusions. Journal of South American Earth Sciences, 8, 267-288.

Van Schmus W.R. Brito Neves B.B., William I.S., Hackspacher P.C., Fetter A.H, Dantas E.L., Babinski M. 2003. The Seridó Group of NE Brazil, a late Neoproterozoic pré- to syn-collisional basin in West Gondwana: insights from SHIRIMP U-Pb detrital zircons ages and Sm-Nd crustal residence (TDM) ages. Precambrian Research, 127, 287-386.

Zucchetti M. 2007. Rochas máficas do Supergrupo Grão Pará e sua relação com a mineralização de ferro dos depósitos N4 e N5, Carajás (PA). PhD Thesis, Departamento de Geologia, Universidade Federal de Minas Gerais, Belo Horizonte, 125 p.